








© The Author(s), 2023. Published by Cambridge University Press on behalf of University of Arizona. This is an Open Access article, distributed under the terms of the Creative Commons Attribution licence (<http://creativecommons.org/licenses/by/4.0/>), which permits unrestricted re-use, distribution and reproduction, provided the original article is properly cited.

MARINE RADIOCARBON CALIBRATION IN POLAR REGIONS: A SIMPLE APPROXIMATE APPROACH USING MARINE20

T J Heaton^{1*}  • M Butzin^{2,3*}  • E Bard⁴  • C Bronk Ramsey⁵  • K A Hughen⁶  • P Köhler³  • P J Reimer⁷ 

¹Department of Statistics, School of Mathematics, University of Leeds, Leeds LS2 9JT, UK

²MARUM-Center for Marine Environmental Sciences, University of Bremen, Bremen, Germany

³Alfred-Wegener-Institut Helmholtz-Zentrum für Polar -und Meeresforschung (AWI), D-27515 Bremerhaven, Germany

⁴CEREGE, Aix-Marseille University, CNRS, IRD, INRAE, Collège de France, Technopole de l'Arbois BP 80, 13545 Aix en Provence Cedex 4, France

⁵Research Laboratory for Archaeology and the History of Art, University of Oxford, 1 South Parks Road, Oxford OX1 3TG, UK

⁶Marine Chemistry and Geochemistry, Woods Hole Oceanographic Institution, Woods Hole, MA 02543, USA

⁷The ¹⁴CHRONO Centre for Climate, the Environment and Chronology, Geography, Archaeology and Palaeoecology, Queen's University Belfast BT7 1NN, UK

ABSTRACT. The Marine20 radiocarbon (¹⁴C) age calibration curve, and all earlier marine ¹⁴C calibration curves from the IntCal group, must be used extremely cautiously for the calibration of marine ¹⁴C samples from polar regions (outside ~ 40°S–40°N) during glacial periods. Calibrating polar ¹⁴C marine samples from glacial periods against any Marine calibration curve (Marine20 or any earlier product) using an estimate of ΔR , the regional ¹⁴C depletion adjustment, that has been obtained from samples in the recent (non-glacial) past is likely to lead to bias and overconfidence in the calibrated age. We propose an approach to calibration that aims to address this by accounting for the possibility of additional, localized, glacial ¹⁴C depletion in polar oceans. We suggest, for a specific polar location, bounds on the value of $\Delta R_{20}(\theta)$ during a glacial period. The lower bound $\Delta R_{20}^{\text{Hol}}$ may be based on ¹⁴C samples from the recent non-glacial (Holocene) past and corresponds to a low-depletion glacial scenario. The upper bound, $\Delta R_{20}^{\text{GS}}$, representing a high-depletion scenario is found by increasing $\Delta R_{20}^{\text{Hol}}$ according to the latitude of the ¹⁴C sample to be calibrated. The suggested increases to obtain $\Delta R_{20}^{\text{GS}}$ are based upon simulations of the Hamburg Large Scale Geostrophic Ocean General Circulation Model (LSG OGCM). Calibrating against the Marine20 curve using the upper and lower ΔR_{20} bounds provide estimates of calibrated ages for glacial ¹⁴C samples in high- and low-depletion scenarios which should bracket the true calendar age of the sample. In some circumstances, users may be able to determine which depletion scenario is more appropriate using independent paleoclimatic or proxy evidence.

KEYWORDS: DeltaR, marine calibration, marine reservoir age, Marine20, polar regions.

1 INTRODUCTION

1.1 Marine ¹⁴C Calibration

To aid calibration of radiocarbon (¹⁴C) samples from open-ocean surface marine environments, the IntCal working group regularly produce marine radiocarbon age calibration curves (known as MarineXX, where XX denotes the year in which the calibration curve was produced). The most recent marine calibration curve is Marine20 (Heaton et al. 2020) which has replaced the earlier 1986, 1993, 1998, Marine04, Marine09, and Marine13 curves (Hughen et al. 2004; Reimer et al. 2009, 2013; Stuiver et al. 1986, 1998; Stuiver and Braziunas 1993). The aim of all these marine radiocarbon age calibration curves is to provide a *best estimate* of the global-scale changes in open ocean surface ¹⁴C levels over the past 55,000 years that incorporates the oceanic smoothing of atmospheric ¹⁴C-age variations and accounts for large-scale paleoclimatic, paleoceanographic, and carbon cycle changes. To enable consistent calibration of marine ¹⁴C samples, the community typically make the significant simplification that any further localized changes in surface ocean depletion are

*Joint 1st authors. Emails: t.heaton@leeds.ac.uk; mbutzin@marum.de



approximately constant over time, and that the global-scale changes modeled within the MarineXX curves capture the main temporal variations in oceanic ^{14}C depletion (Heaton et al. 2022).

In polar regions such a simplification cannot however be justified. At high-latitudes, during glacial periods, we expect there may have been significant additional localized changes in surface-water ^{14}C concentration (Butzin et al. 2005) that are not captured by the global-scale MarineXX curves. These temporal changes, to what is known as the regional $\Delta R(\theta)$, make the calibration of marine ^{14}C samples from such polar regions particularly challenging. Without adjustment to account for potential variations over time in polar $\Delta R(\theta)$, none of the MarineXX curves should be used for calibration of marine ^{14}C samples from polar regions in glacial periods. If we do not account for such temporal changes in $\Delta R(\theta)$ it is likely we will obtain calibrated age estimates for polar ^{14}C samples in glacial periods that are spuriously precise and biased towards being older than their true calendar ages.

Before the impact of anthropogenic emissions, the concentration of ^{14}C in the surface ocean has always been depleted compared with the level of ^{14}C in the contemporaneous atmosphere. Oceanic ^{14}C levels also show a smoother response to ^{14}C production changes than the atmosphere: variations in ^{14}C -age (and $\Delta^{14}\text{C}$) over time are damped in the oceans compared to the atmosphere (Levin and Heshaimer 2000). We measure the overall surface ocean ^{14}C depletion, at any location and time, via the marine reservoir age (MRA). This MRA, denoted $R^{\text{Location}}(\theta)$, defines the difference, at calendar age θ cal yr BP, between the radiocarbon age of dissolved inorganic carbon in the mixed ocean surface layer at that location, and the radiocarbon age of CO_2 in the Northern Hemispheric (NH) atmosphere (Stuiver et al. 1986).

The overall MRA, $R^{\text{Location}}(\theta)$, in a particular location is influenced by both *global-scale* factors and *local-scale* factors (Bard 1988; Stuiver and Braziunas 1993):

$$R^{\text{Location}}(\theta) = R^{\text{GlobalAv}}(\theta) + \Delta R^{\text{Location}}(\theta).$$

Here, $R^{\text{GlobalAv}}(\theta)$ captures the *global-scale* MRA effects; and $\Delta R^{\text{Location}}(\theta)$ the *local-scale* depletion factors. *Global-scale* factors include atmospheric CO_2 (Köhler et al. 2017) and ^{14}C production changes (Reimer et al. 2020), as well as large-scale changes to ocean circulation (e.g., Böhm et al. 2015; Henry et al. 2016; Hodell et al. 2003; Oka et al. 2021) and air-sea gas exchange rates (e.g., Kageyama et al. 2021; Kohfeld et al. 2013; McGee et al. 2010). Crucially, the smoothing of the high frequency atmospheric ^{14}C -age variation which is inherent to the ocean is also predominantly incorporated into this $R^{\text{GlobalAv}}(\theta)$. More *local-scale* effects, which are incorporated through $\Delta R^{\text{Location}}(\theta)$ and might have a further influence on the MRA in a specific area of study, include the depth of the ocean at that location, the presence of sea-ice, regional winds, and coastal upwelling (Key 2001; Key et al. 2004; Reimer and Reimer 2001; Toggweiler et al. 2019).

Notation: The estimates of both $R^{\text{GlobalAv}}(\theta)$ and $\Delta R^{\text{Location}}(\theta)$ are updated with each MarineXX iteration as our knowledge increases. We use a subscript to denote which calibration curve we are referring to, so that $R_{20}^{\text{GlobalAv}}(\theta)$ and $\Delta R_{20}(\theta)$ refer to the Marine20 estimates of *global-scale* and the *local-scale* depletion effects (Heaton et al. 2020). We also drop the location superscript in $\Delta R^{\text{Location}}$ where it is not essential for comprehension. A glossary of the key notation can be found in Table A1 (Appendix A).

1.2 The Marine20 calibration curve and $\Delta R(\theta)$ in polar regions

The Marine20 estimates (and all earlier marine calibration curves) only aim to model the *global-scale* changes in oceanic ^{14}C levels, i.e., $R^{\text{GlobalAv}}(\theta)$. In any specific oceanic location, at any particular time θ , there is expected to be some additional localized ^{14}C variation. This must be accounted for through the $\Delta R(\theta)$ term. While we expect $\Delta R(\theta)$ to vary over time, we do not currently have sufficient knowledge to be able to accurately model these changes or, in most locations, to estimate them with sufficient precision from data (Heaton et al. 2022).

To allow the community to calibrate marine ^{14}C samples, we must therefore make a considerable simplification. The standard approach, taken since the first Marine calibration curve of Stuiver et al. (1986), is to consider $\Delta R(\theta)$ as being approximately constant (or at most to vary slowly) over time, i.e., $\Delta R(\theta) \equiv \Delta R$. We can estimate these regional values, ΔR_{20} in the case of the Marine20 curve, using ^{14}C observations from the recent past. Such reference ^{14}C samples and estimates of ΔR_{20} are available, for example, in the maintained database at <http://calib.org/marine/> (Reimer and Reimer 2001). Having made such a simplification, to calibrate a new ^{14}C sample we subtract the appropriate regional ΔR_{20} from the observed radiocarbon age of the sample, and then calibrate against Marine20.

This approach to calibration, assuming that $\Delta R(\theta) \equiv \Delta R$, is recognized as being a coarse approximation for any ocean location. However, it is seen as a necessary simplification to enable a standardized approach to marine calibration until our knowledge improves (Heaton et al. 2022). However, in polar regions, the assumption of a constant $\Delta R(\theta)$ over time cannot be justified. During glacial periods, outside *ca.* 40°S–40°N, we expect localized sea-ice cover, strong winds, and ocean circulation changes may have had substantial additional short-term effects on $\Delta R(\theta)$ (Butzin et al. 2005; Völker and Köhler 2013). Pre-Holocene/glacial values of $\Delta R(\theta)$ may therefore be considerably larger than the values of $\Delta R(\theta)$ during the Holocene/recent past (Butzin et al. 2017; Skinner et al. 2019).

When calibrating ^{14}C samples that arise from marine locations outside *ca.* 40°S–40°N and are older than *ca.* 11.5 cal kyr BP, it is therefore not appropriate to calibrate against any MarineXX curve using a value of ΔR estimated from Holocene/recent past samples. If we fail to take the potentially increased $\Delta R(\theta)$ into account during calibration, we are likely to introduce substantial biases in the resultant calendar age estimates: providing estimates for the calendar ages of glacial-period marine ^{14}C samples in polar regions that are significantly older than their true calendar ages, and which underestimate the calendar age uncertainty.

Glacial increases in $\Delta R(\theta)$ at high-latitudes are predominantly driven by the increased coverage of sea-ice in these polar regions. Sea-ice restricts air-sea gas exchange, hence slowing the uptake of new atmospheric $^{14}\text{CO}_2$ into the surface ocean. It is commonly assumed that sea-ice is impermeable for $^{14}\text{CO}_2$, and that formation and melting of sea-ice do not change the concentration of dissolved inorganic ^{14}C in the surface ocean. Under these assumptions, all air-sea exchange will vanish in fully ice-covered areas and the ^{14}C concentrations of the surface water will reflect the greater depletion of deeper or remote waters. While we are able to model the effect of sea-ice on surface ocean ^{14}C depletion, we lack sufficient knowledge over the glacial period on the appropriate climate scenario (and the extent of sea-ice at high latitudes) to use for that modeling. Over the course of the glacial, the climate and the extent of sea-ice are not expected to remain constant but rather to vary substantially over time.

Location-specific estimates of the overall open-ocean surface water ^{14}C depletion (i.e., $R^{\text{Location}}(\theta)$, the total MRA) are available under fixed carbon cycle and climate scenarios via the Hamburg Large Scale Geostrophic Ocean General Circulation Model (LSG OGCM, discussed in Butzin et al. 2020) at <https://doi.pangaea.de/10.1594/PANGAEA.914500>. In principle, these LSG OGCM estimates could be used for polar ^{14}C calibration, by adjusting the IntCal20 curve. However, the LSG OGCM scenarios provided are not transient, in terms of climate, and so calibrating under any individual scenario will still lead to overconfidence in the resultant age estimate. Further, the limited spatial resolution of the LSG OGCM means that estimation of a further regional depletion term, a ΔR^{LSG} , is still required. Direct calibration using the LSG OGCM estimates is therefore non-trivial using current software.

1.3 A Simple Recommendation for Marine Polar ^{14}C Calibration

In this paper, we suggest how a user might calibrate high latitude (outside *ca.* 40°S–40°N) marine ^{14}C samples in such a way as to reduce the potential for bias and overconfidence in the resultant calendar age estimates. Since detail on past polar climate and the extent of sea-ice is largely unknown, and as we wish to retain simplicity in calibration, our proposal is, by necessity, a coarse approximation. We suggest modifying the $\Delta R(\theta)$ used for calibration dependent upon whether the sample arose during glacial, or Holocene/interglacial, conditions. Our suggestion is informed by the LSG OGCM scenarios while still retaining use of the Marine20 curve.

The application of a glacial increase in $\Delta R(\theta)$ will have the effect of shifting the calibrated age estimate towards more recent dates. Hence, to determine if the ^{14}C sample potentially lies in the glacial, we can calibrate first using just the lower depletion approach (see Section 1.3.1) with a modern-day ΔR_{20} . If this (low-depletion) calibration provides a calendar age date which falls in the glacial period, then the calibration user should also perform an additional calibration as this sample may require a glacial $\Delta R(\theta)$ increase (described in Section 1.3.2).

Note that while we use the term Holocene/glacial to denote the partition between the two suggested calibration approaches, we do not provide a precise calendar date as to when substantial changes in polar $\Delta R(\theta)$ may have occurred. This decision, and the glacial boundary, should be made and justified by the calibration user, drawing on various lines of paleoclimatic-paleoceanographic evidence.

1.3.1 Calibrating polar ^{14}C samples from the Holocene (*ca.* 11,500–0 cal yr BP)

We suggest that those users calibrating polar ^{14}C samples from the Holocene can calibrate directly against Marine20 using a standard estimate of ΔR_{20} obtained via ^{14}C samples from the Holocene (e.g., ^{14}C samples from the recent past). This suggestion is based on the relatively stable climate during the Holocene period and an assumption that, even at high latitudes, we would not expect substantial sea-ice based temporal variations in $\Delta R(\theta)$. Such a ΔR_{20} estimate can be obtained using samples from the recent past via the maintained database at <http://calib.org/marine/> (Reimer and Reimer 2001) or from paired radiocarbon dated marine/terrestrial samples. During the Holocene, the approach to calibration of polar samples therefore remains the same as that traditionally taken for any other marine location. This retains consistency.

If this calibration, with a Holocene-based estimate of ΔR_{20} , provides an estimate for the calendar age which lies entirely in the Holocene, then we can be confident the sample arises from this period. The user can then stop after this single calibration and report their calibrated age interval. However, if the calibrated age extends into the glacial (beyond approximately

11,500 cal yr BP), the sample may require a glacial polar $\Delta R(\theta)$ boost and the user should follow Section 1.3.2.

Note: We recognize that there is a scarcity of modern ΔR_{20} values in the maintained <http://calib.org/marine/> database for some specific regions and locations. In regions without substantial vertical ocean mixing, we suggest that users may consider the origin of the ocean surface water based upon the currents involved and select a ΔR_{20} based on the appropriate values in those origins. Information on currents can be obtained through the Ocean Current Regimes tab within the <http://calib.org/marine/> database.

1.3.2 Calibrating polar ^{14}C samples from glacial periods (ca. 55,000–11,500 cal yr BP)

For those users wishing to calibrate high-latitude samples from glacial periods, we propose the application of a latitude-dependent adjustment to the value of ΔR_{20} . This adjustment aims to account for potential glacial changes in regional ^{14}C depletion within polar oceans due to localized sea-ice and other local factors. Specifically, during glacial periods, we suggest that a user consider two distinct ΔR_{20} polar depletion scenarios providing bracketing glacial climates:

1. Minimal polar ^{14}C glacial depletion—Calibrate against Marine20 applying a $\Delta R_{20}^{\text{Hol}}$ that matches the adjustment for regional ^{14}C depletion seen during the Holocene. As for Section 1.3.1, this $\Delta R_{20}^{\text{Hol}}$ can be calculated using ^{14}C samples from the recent past such as those found in the maintained database at <http://calib.org/marine/> (Reimer and Reimer 2001).
2. Maximal polar ^{14}C glacial depletion—Apply an increase to the Holocene-based $\Delta R_{20}^{\text{Hol}}$ to obtain a high-depletion $\Delta R_{20}^{\text{GS}} = \Delta R_{20}^{\text{Hol}} + \Delta R_{20}^{\text{Hol} \rightarrow \text{GS}}$ that is chosen to provide optimal agreement with the GS scenario of the LSG OGCM. Calibrate against Marine20 using this increased $\Delta R_{20}^{\text{GS}}$.

The proposed increase, i.e., $\Delta R_{20}^{\text{Hol} \rightarrow \text{GS}}$, that is required to transform $\Delta R_{20}^{\text{Hol}}$ into $\Delta R_{20}^{\text{GS}}$ is dependent upon the latitude of the sample. The values of $\Delta R_{20}^{\text{Hol} \rightarrow \text{GS}}$ at each latitude are shown in Figure 1, with the values tabulated in Table A2 (Appendix A) and available as an Excel spreadsheet in Supplementary Information D. Calibrating against Marine20 first with the low-depletion $\Delta R_{20}^{\text{Hol}}$ adjustment, and then separately with the high-depletion $\Delta R_{20}^{\text{GS}}$ scenario, should hopefully provide bracketing calibrated ages for the true calendar age of the sample.

Such an approach retains simplicity in calibration, allowing use of Marine20 and existing calibration software. A user is not required to create their own (location-specific) calibration curve since the proposed approach requires only an adjustment to ΔR_{20} . This is typically available as an option in calibration software. Our suggested adjustment from $\Delta R_{20}^{\text{Hol}}$ to $\Delta R_{20}^{\text{GS}}$ depends only upon the latitude of the ^{14}C sample we wish to calibrate (and not its specific longitude or ocean basin).

1.3.3 Additional considerations

Our current approach is only intended as a first approximation and hence is designed to be coarse. There is much that we still do not know about ^{14}C levels at high-latitudes and our primary aim is to make users aware they must tread carefully when using calibrated dates based on ^{14}C marine samples in polar regions. As we learn more about the past climatic conditions, we expect we will be able to provide more localized, detailed, and temporally varying adjustments to $\Delta R_{20}(\theta)$.

In particular, due to the separation of the Pacific from the Atlantic and Arctic Ocean during the last glacial by a sea level drop that allowed the crossing of the Bering Strait on land (De Boer

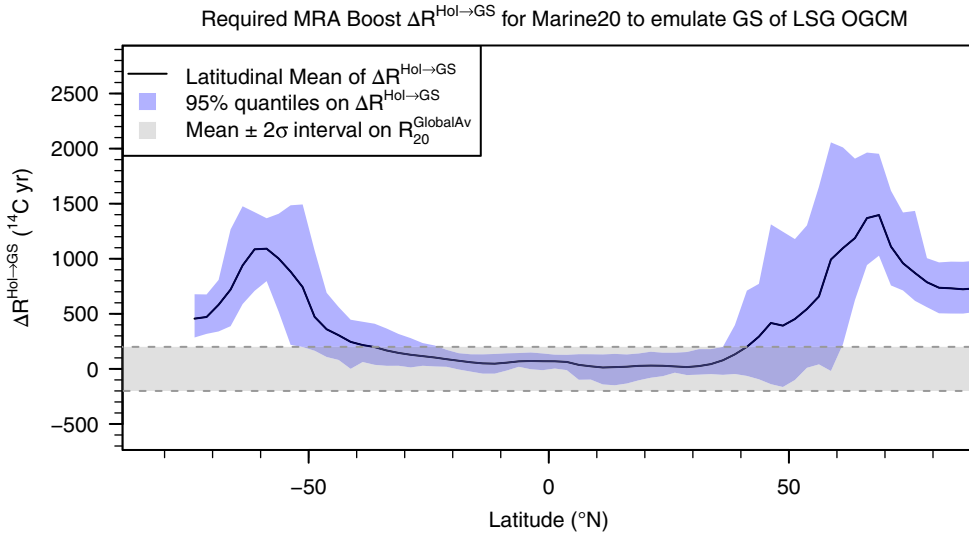


Figure 1 The latitudinal-average increase in oceanic ^{14}C depletion, $\Delta R_{20}^{\text{Hol} \rightarrow \text{GS}}$, needed to transform from Marine20 (with an initial Holocene $\Delta R_{20}^{\text{Hol}}$) to the localized GS scenario estimates of the LSG OGCM. The shaded gray area represents the mean width (from 40,000–11,500 cal yr BP) of the $\pm 2\sigma$ uncertainty on Marine20's $R_{20}^{\text{GlobalAv}}(\theta)$. The blue shaded area represents the 95% quantiles on the $\Delta R_{20}^{\text{Hol} \rightarrow \text{GS}}$ shift required for the given latitude. (Please see online version for color figures.)

and Nof 2004; Jakobsson et al. 2017; Knudson and Ravelo 2015), we expect an ocean-basin dependent adjustment may be appropriate. For this study, we did investigate such a dependence (see Supplementary Information B and C, Figures S2 and S6) but felt that basin-specific adjustments would provide potentially spurious precision as they were predominantly due to model choice (in particular, the positioning of sea-ice).

We also note that some users may have independent paleoclimatic evidence as to the glacial conditions in their oceanic location, for example through proxy evidence within a sediment core. For such users, we still recommend they present our bracketing approach (i.e., both limiting depletion scenarios). However, they may then wish to use their expert knowledge to argue for one scenario as being more appropriate than the other (or indeed for an intermediate level of ^{14}C depletion lying between the two low- and high- depletion extremes). With rigorous palaeoclimatic proxies, it may even be possible to scale the appropriate $\Delta R_{20}(\theta)$ to apply to each sample between the extreme $\Delta R_{20}^{\text{Hol}}$ and $\Delta R_{20}^{\text{GS}}$ values. This offers the possibility to provide more precise calibrated age ranges.

Finally, we advise users to interpolate the boost $\Delta R_{20}^{\text{Hol} \rightarrow \text{GS}}$ for those latitudes not explicitly provided in Table A2 (Appendix). This will ensure smooth changes to calibrated ages. Those considering marine ^{14}C samples that span a latitudinal range (e.g., from feeding birds) should create their $\Delta R_{20}^{\text{Hol} \rightarrow \text{GS}}$ boost by averaging over that latitudinal range.

1.4 Paper Layout

The paper is set out as follows. In Section 2, we provide a short explanation of Marine20 (Heaton et al. 2020) which provides estimates of global $R_{20}^{\text{GlobalAv}}(\theta)$ MRA effects. We then compare these to localized model estimates for open-ocean surface water ^{14}C depletion from

the LSG OGCM (Butzin et al. 2020) under three different scenarios (PD, GS and CS). We show how we can approximately transition from the global Marine20 to the various localized LSG OGCM estimates by applying a constant shift to $R_{20}^{GlobalAv}(\theta)$.

In Section 3, we summarize these shifts from Marine20's $R_{20}^{GlobalAv}(\theta)$ to obtain our suggested latitudinal increases $\Delta R_{20}^{Hol \rightarrow GS}$. These allow us to approximate the GS scenario of the LSG OGCM using the Marine20 curve. To further support our proposed bracketing approach, we compare the upper and lower bounds for $R^{Location}(\theta)$ obtained via our recommended adjustments to Marine20's global-scale $R_{20}^{GlobalAv}(\theta)$ against directly observed surface MRA estimates at the site of the deep-sea core MD04-2829 (59.0°N, 9.5°W; Skinner et al. 2019).

We present worked examples of polar ocean ^{14}C calibration using our bracketing approach in Section 4. We consider the calibration of individual samples as well as the construction of an age-depth model using deep-sea core MD02-2496 offshore of Vancouver Island at 49.0°N, 127.0°W (Cosma et al. 2008; Taylor et al. 2014). In this Section, we also briefly discuss how individuals might present their calibrated dates when they have independent proxy information on the appropriate depletion scenario. Finally in Section 5, we summarize our recommendations and describe avenues for future work.

2 ADJUSTING MARINE20'S $R^{Global}(\theta)$ TO MATCH REGIONAL LSG OGCM OUTPUT

2.1 Marine20 vs. LSG OGCM

Marine20 uses a transient application of the BICYCLE carbon cycle box model (Köhler et al. 2006, 2010). While Marine20 does incorporate the major changes in the global carbon cycle that occurred during the glacial, it only aims to summarize their wide-scale effect on large ocean areas. The resultant Marine20 curve, and its $R^{Global}(\theta)$, should therefore only be viewed as providing a *global-scale* estimate of changes over time in oceanic ^{14}C levels (Heaton et al. 2020, 2022). If there are additional localized effects in a study location that are temporally varying, for example, if regional sea-ice was not present during the Holocene but likely extensive during the glacial, then a Marine20 user must incorporate those effects through adjustments to the regional $\Delta R(\theta)$.

The LSG OGCM (Butzin et al. 2020) is able to provide more localized ocean modeling, generating estimates of ^{14}C levels and MRA at specific marine locations on a 2.5° by 2.5° grid (see Figure 2). However, the LSG OGCM is much slower to run than BICYCLE. The LSG OGCM estimates are run under fixed climate scenarios as well as being model-specific. This currently makes it difficult to use the LSG OGCM to fully understand the uncertainties in local MRAs since knowledge regarding the appropriate glacial climate and carbon cycle to apply is highly imprecise. LSG OGCM estimates of overall MRA are available, forced by the IntCal20 posterior mean for atmospheric ^{14}C concentrations (Reimer et al. 2020), under three specific climate scenarios (Butzin et al. 2005):

- PD—a climate scenario intended to be very similar to the present day.
- GS—a glacial climate scenario representing the Last Glacial Maximum (LGM), featuring a shallower AMOC weakened by about 30% compared to PD.
- CS—a more extreme glacial climate scenario aiming to mimic cold stadials with further AMOC weakening by about 60% compared with PD.

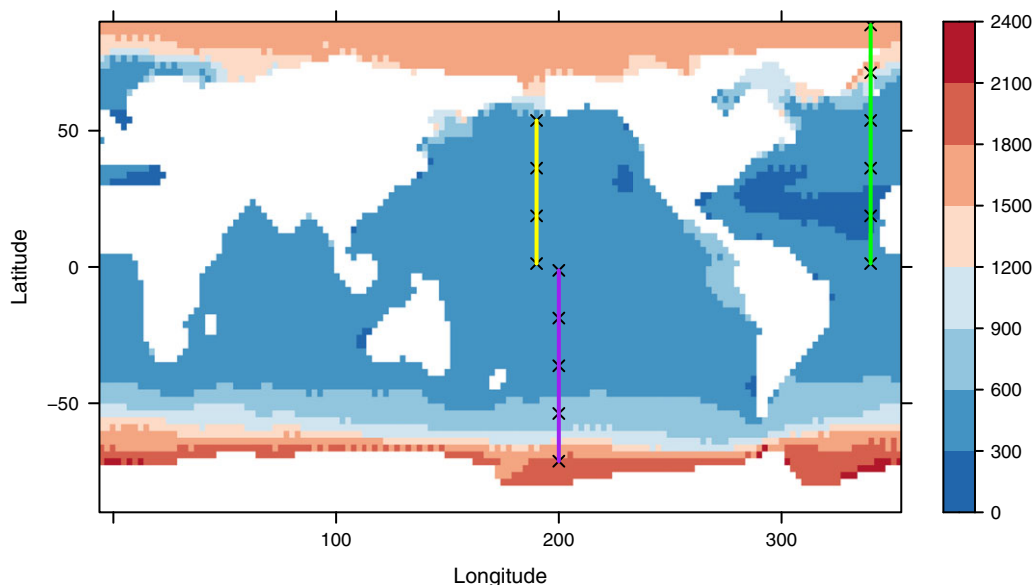


Figure 2 Location-specific estimates, at 0 cal yr BP, of the overall MRA, $R^{Location}(\theta)$, obtained by the LSG OGCM under the PD scenario. The plotting color represents the MRA value with scale shown on RHS (in ^{14}C yrs); white represents land. Three line transects are shown passing through the South Pacific (purple 160°W), North Pacific (yellow 170°W), and North Atlantic and Arctic (green 20°W). We highlight sample sites on each transect which are used later (in Figure 3) to illustrate the potential changes in surface-water ^{14}C depletion under various glacial scenarios as we extend into higher-latitude oceans.

While designed to incorporate more of the localized variations in surface-ocean ^{14}C depletion, the LSG OGCM estimates do not incorporate every potential influence and are model specific. Consequently, they still require a regional correction ΔR^{LSG} (equivalent to a ΔR_{20}) if they are to be used for calibration. This ΔR^{LSG} would typically be obtained by comparing known-age ^{14}C samples from the recent past against the corresponding PD scenario output from the nearest open-ocean LSG OGCM location (analogous to the calculation of a ΔR_{20}). Using the LSG OGCM outputs directly for calibration is therefore non-trivial; and since they are run under fixed climate scenarios, calibration against any one scenario will still give overprecise calendar ages. However, we believe that the constant-state GS scenario provides a reasonable upper bound for the level of oceanic ^{14}C depletion during the glacial. More detail on both construction of the BICYCLE/Marine20 and the LSG OGCM estimates can be found in Supplementary Information A.

To justify our proposed approach to polar calibration using Marine20, we demonstrate that a user can approximately recreate the regional LSG OGCM estimates while maintaining use of the *global-scale* Marine20 through a simple modification, or boost, to their $\Delta R_{20}(\theta)$. Our approach relies on three key elements. Firstly, that each climate scenario of the LSG OGCM output can be approximated by applying a constant (not time dependent) shift to Marine20's $R_{20}^{Global}(\theta)$. Consequently, we can effectively transition to the different LSG OGCM scenarios, while retaining the use of Marine20, just by applying a static (constant) shift to a present-day estimate of ΔR_{20} . Secondly, in low-latitude locations (within 40°S to 40°N) the uncertainty bands on Marine20 already encapsulate the LSG OGCM scenarios. Thirdly, that by latitudinally averaging the boost required to match the LSG OGCM scenario, we reduce the

influence of the model specificity of the LSG OGCM (for example, the precise location and dynamics of sea-ice and freshwater balance) and simplify the application of our proposed calibration approach.

We propose using the GS scenario of the LSG OGCM as the upper bound for surface ocean ^{14}C depletion in the glacial. However, should a user decide that they wish to bound their glacial climate with the more extreme CS scenario, a similar set of findings hold. The corresponding CS-based upper bound on the glacial boost to ΔR_{20} can be found in Table A2 (Appendix) and the Supplementary Information (Figures S3–S6 in Supplementary Info C, and accompanying spreadsheet in Supplementary Info D).

2.2 Illustrative Regional Estimates of MRA

The LSG OGCM surface-water estimates are provided every 50 cal yrs for open ocean regions. For both the GS and CS scenarios, the Pacific was disconnected from the Arctic Ocean because the Bering Strait (which is currently shallower than 50 m in depth) was closed during the glacial sea-level lowstand (Jakobsson et al. 2017). Global sea-levels during the glacial are believed to have been in the order of 130m lower than those of the present day (Lambeck et al. 2014).

To illustrate our proposed approach, we consider three transects (Figure 2). The first (in purple) passes through the Southern Pacific Ocean at a longitude of 160°W . The second (in yellow) through the Northern Pacific at a longitude of 170°W . During the glacial period this transect becomes cut-off from the Arctic Ocean further North by closure of the Bering Strait. The third transect (in green) passes through the Atlantic and into the Arctic at a longitude of 20°W . The estimates along these transects are typical of the LSG OGCM outputs. In Figure 2, we plot the spatial MRA estimates provided by the LSG OGCM under the PD scenario at 0 cal yr BP (i.e., 1950 CE).

To enable comparison of the LSG OGCM estimates with Marine20 we must account for the shifts (denoted ΔR^{LSG} and ΔR_{20} respectively) that would need to be applied to each estimate. For each location, we have calculated the difference between the mean (in ^{14}C yrs) of the PD scenario of the LSG OGCM from 11,500–0 cal yr BP and the mean of the $R_{20}^{GlobalAv}(\theta)$ in the same period. This difference has then been used to shift both the PD and GS outputs of the LSG OGCM for that location. Figure 3 presents these *shifted* location-specific estimates of the MRA over time along the three selected transects under both the PD and GS scenario of the LSG OGCM; and the equivalent estimates with Marine20. For each location, the mean over the 11,500–0 cal yr BP period of $R_{20}^{GlobalAv}(\theta)$ and the shift-adjusted PD outputs of the LSG OGCM are equal. Applying such a shift to both the PD and GS outputs of the LSG OGCM enables comparison between the calibration one would achieve using Marine20 (with a constant estimate of ΔR_{20} based on recent-past/Holocene ^{14}C data), and that obtained using the LSG OGCM outputs (with a constant ΔR^{LSG} based on the same recent-past/Holocene ^{14}C data). We do not show the GS estimates from 11,500–0 cal yr BP as this climate scenario is inappropriate for the Holocene.

Figure 3 effectively illustrates the difference, at a specific location, in overall MRA one would obtain using Marine20 compared with the PD and GS scenarios of the LSG OGCM. The difference between the PD (colored solid lines) and GS (dashed lines) estimates between 55,000–11,500 cal yr BP show how much additional ^{14}C depletion, according to the LSG OGCM, is modeled at that ocean location by changing from a Holocene-type (PD) scenario to a glacial (GS) scenario. The difference between the $R_{20}^{GlobalAv}(\theta)$ of Marine20 (solid black line)

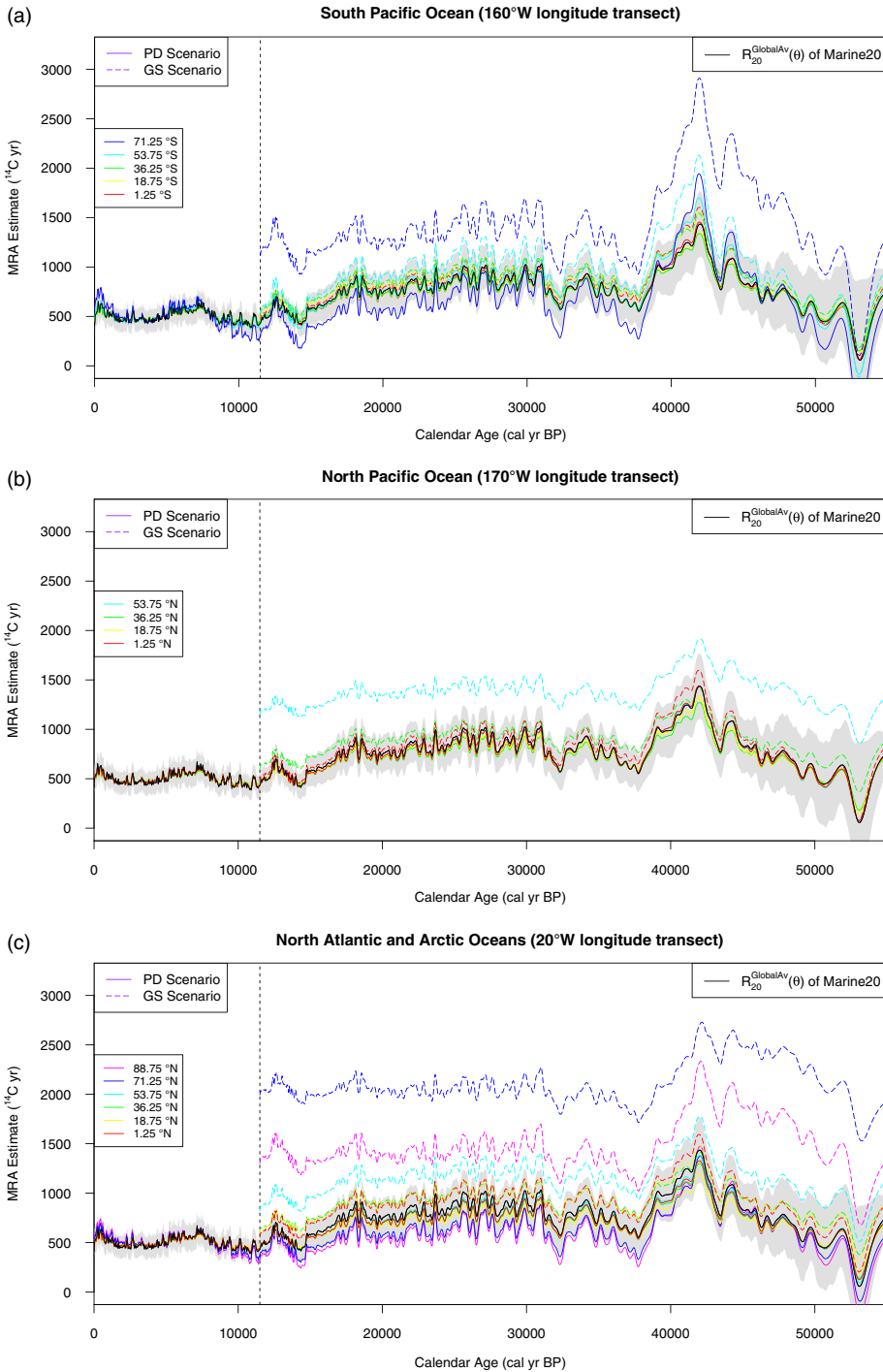


Figure 3 Comparing the Marine20, PD and GS estimates for the MRA at marine locations along the line transects shown in Figure 2 passing through the: (a) South Pacific Ocean; (b) North Pacific Ocean; (c) North Atlantic and Arctic Oceans. Shown in black is the estimate of $R_{20}^{\text{GlobalAv}}(\theta)$ used in Marine20 together with its 2σ interval (gray shaded region). The GS and PD estimates from the LSG OGCM have been shifted so that the mean of the plotted PD scenario in each location agrees with the mean of $R_{20}^{\text{GlobalAv}}(\theta)$ from 11,500–0 cal yr BP. The shifted PD scenario for each latitude on the transect is shown as a (variously colored) solid line and the shifted GS scenario as a matched dashed line. The vertical line represents 11,500 cal yr BP. GS estimates from the LSG OGCM are not provided for calendar ages more recent than this.

and the adjusted GS estimates show how much additional localized ^{14}C depletion might have occurred, beyond that already incorporated within the *global-scale* estimate of Marine20, under a GS glacial scenario. These location-dependent increases from $R_{20}^{\text{GlobalAv}}(\theta)$ must be incorporated into $\Delta R_{20}(\theta)$ if we wish to represent the GS scenario with Marine20. Similar plots for the more extreme CS scenario of the LSG OGCM can be found in the Supplementary Information C (Figures S3 and S4).

2.3 Comparing the LSG OGCM and Marine20

Several observations are immediately apparent from Figure 3. Firstly, during the Holocene, once we have estimated both a ΔR_{20} and a ΔR^{LSG} regional/coastal adjustment based on modern ^{14}C samples, the PD scenario from the LSG OGCM provides very similar MRA estimates to Marine20 for all the ocean locations on our sample transects. As we extend into the very high latitudes in the Southern Pacific and Arctic Ocean, the PD scenario does perhaps suggest slightly greater variations in MRA, in terms of the change from the levels of ^{14}C depletion seen at the beginning of the Holocene compared to the present day, than Marine20. However, these changes are minor and generally lie within the uncertainty bands of Marine20. Intuitively, the uncertainty bands of Marine20 result from considering multiple potential climate and carbon cycle scenarios. It is likely that, during the Holocene, one of these (BICYCLE-based) scenarios lies extremely close to the PD scenario of the LSG OGCM. Consequently, for samples between 11,500–0 cal yr BP, there should be little difference between calibrating at sites along our transects using the PD output from LSG OGCM (with a ΔR^{LSG} adjustment) and using Marine20 (with a regional ΔR_{20}). This is the case for both polar and equatorial regions.

Secondly, from 55,000–11,500 cal yr BP, we can see that (after the ΔR_{20} and ΔR^{LSG} shift/adjustment) the PD scenario of the LSG OGCM (colored solid lines) tends to generate estimates of the overall MRA along our transects that are lower than those of Marine20 (solid black line). This highlights that, while not able to resolve regionally, Marine20 does incorporate global effects of climatic and carbon cycle changes during the glacial. In this pre-Holocene period, the PD scenario of the LSG OGCM is unlikely to be appropriate as we know there were substantial global changes in the climate and carbon cycle between the glacial and the present day (Böhm et al. 2015; Henry et al. 2016; Kageyama et al. 2021; Oka et al. 2021; Petit et al. 1990). We expect that, from 55,000–11,500 cal yr BP, the true level of oceanic ^{14}C depletion at a site will therefore be bounded below by the (ΔR_{20} -adjusted) Marine20 rather than the (ΔR^{LSG} -adjusted) PD scenario of the LSG OGCM.

Thirdly, if we consider the (ΔR^{LSG} -adjusted) GS scenario estimates (dashed lines) as providing an upper bound on the overall level of ^{14}C depletion at any marine site then, for the more equatorial locations, these are encapsulated in Marine20's 2σ uncertainty bands (shaded gray). Only once we extend beyond approximately 40°S or 40°N do the (ΔR^{LSG} -adjusted) GS scenario of the LSG OGCM provide location-specific estimates of overall MRA that are not covered by the tail estimates one would obtain with (a ΔR_{20} -adjusted) Marine20. This suggests that on our transects, for calibration of marine samples from regions within $\sim 40^\circ\text{S}$ – 40°N , the use of Marine20 (with a modern day ΔR_{20}) can be justified back to 55,000 cal yr BP as its inbuilt uncertainty will cover the upper (GS-scenario) limit for regional ^{14}C depletion. However, at higher latitudes, the GS scenarios indicate the possibility of substantial additional localized ^{14}C oceanic depletion during glacial periods that is not captured in the global scale Marine20. Under the GS scenario, along our transects, the overall MRA in high-latitude polar regions may be increased by up to 1000 ^{14}C yrs during the glacial compared to the global Marine20

values. To recreate this GS scenario, these polar-specific increases would need to be accounted for by a corresponding change to $\Delta R_{20}(\theta)$ if Marine20 is used for calibration.

Fourthly, Figure 3 suggests that from 40,000–11,500 cal yr BP the increase in a particular location from the Marine20-based estimate of overall MRA to the LSG OGCM under its GS scenario (after the initial ΔR_{20} and $\Delta R_{20}^{\text{LSG}}$ adjustments) is approximately constant over time. This can be seen very clearly in Figure S1 of the Supplementary Information B where we present the increase for each location along our three selected ocean transects. For a given location, we can therefore get a good approximation of the overall MRA estimate under the GS scenario of the LSG OGCM (at least between 40,000–11,500 cal yr BP) with Marine20 by applying a constant (albeit location-specific) increase to ΔR_{20} . These increases (latitudinally averaged rather than along single transects) will become our $\Delta R_{20}^{\text{Hol} \rightarrow \text{GS}}$.

3 ADJUSTMENTS TO RECREATE A GLACIAL LSG OGCM SCENARIO USING MARINE20 FROM 55,000–11,500 CAL YR BP

3.1 Summarizing the High-Latitude Increases in Regional ^{14}C Depletion for a Glacial Scenario

To provide an upper (maximum) bound on the additional regional ^{14}C depletion that may need to be incorporated into Marine20's $\Delta R_{20}(\theta)$ at high-latitudes during glacial periods, we have calculated latitudinal-average $\Delta R_{20}^{\text{Hol} \rightarrow \text{GS}}$ adjustments. These adjustments take the form described in Section 2 where, for every marine location on the 2.5° by 2.5° grid of the LSG OGCM grid, we have:

- Shifted the LSG OGCM estimates so that the PD scenario in that location has a mean during the period from 11,500–0 cal yr BP that matches Marine20's $R_{20}^{\text{GlobalAv}}(\theta)$.
- Calculated the difference in the mean, during the glacial period from 40,000–11,500 cal yr BP, between $R_{20}^{\text{GlobalAv}}(\theta)$ and the (shifted) GS scenario.

This difference indicates by how much the level of ^{14}C depletion must be increased from the global-only $R_{20}^{\text{GlobalAv}}(\theta)$ to recreate the regional GS scenario of the LSG OGCM. At a given latitude, we summarize the mean (and 95% quantiles) of these increases to obtain the latitude-dependent $\Delta R_{20}^{\text{Hol} \rightarrow \text{GS}}$ values shown in Figure 1 (and Figure 4 showing the adjustment required at a particular latitude).

Note that we perform latitudinal averaging, rather than providing latitude and longitude dependent adjustments, to reduce the effect of model specificity in the LSG OGCM estimates regarding precise sea-ice location/dynamics and freshwater balance. We also do not provide, or suggest using, the variance on the shifts at a given latitude. The set of modeled values provided by the LSG OGCM at a given latitude are not well approximated by a normal distribution. To recreate the GS scenario, we propose simply applying the mean shift $\Delta R_{20}^{\text{Hol} \rightarrow \text{GS}}$ at a given latitude and leaving the uncertainty as for the Holocene-based ΔR_{20} .

We also calculate the shift needed based on the period from 40,000–11,500 cal yr BP, to avoid the non-constancy in the differences from the LSG OGCM outputs to Marine20 at high latitudes from 55,000–40,000 cal yrs BP when atmospheric ^{14}C levels increased very rapidly (Reimer et al. 2020). We suggest our calculated shifts can however be applied back to 55,000 cal yr BP, although at very high latitudes, users should recognize additional adjustments may be needed for ^{14}C samples of such great age.

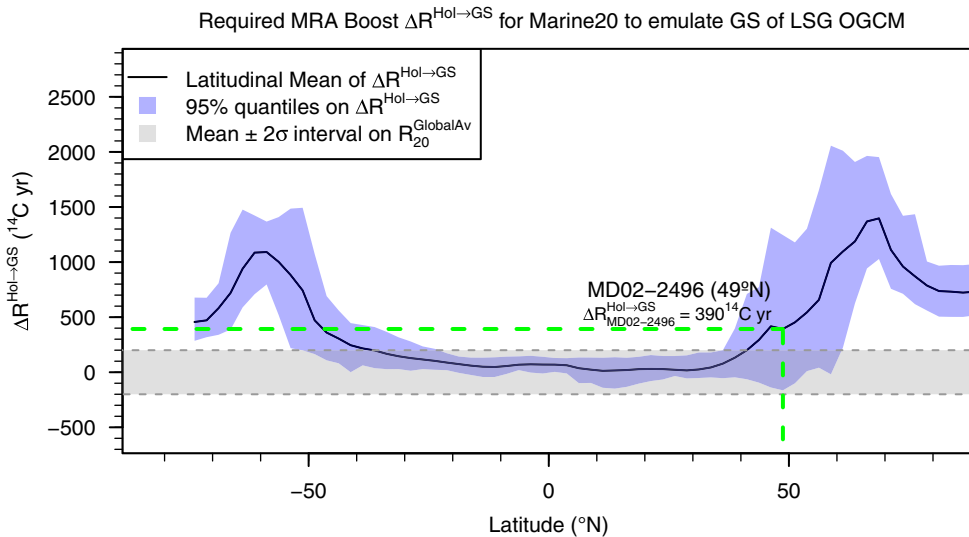


Figure 4 The latitudinal-average increase $\Delta R_{20}^{Hol \rightarrow GS}$ needed to recreate the GS scenario of the LSG OGCM from Marine20 during the glacial time period (reproducing earlier Figure 1). To estimate the adjustment needed at a particular location, e.g., core site MD02-2496 at 49°N, we read the value for the corresponding latitude. Here, the required boost $\Delta R_{MD02-2496}^{Hol \rightarrow GS}$ to recreate the GS scenario using Marine20 (to be added to an initial Holocene ΔR_{20}^{Hol} estimate) is ca. 390 ^{14}C yrs.

For more equatorial ocean locations, the increase $\Delta R_{20}^{Hol \rightarrow GS}$ is seen to overlap with the uncertainty bands on $R_{20}^{GlobalAv}(\theta)$. For these low-latitude regions, within ca. 40°S–40°N, we therefore suggest that no artificial boosting of (a Holocene-based) ΔR_{20} in glacial periods is required. A user can (cautiously) calibrate ^{14}C samples into the glacial period using an estimate of ΔR_{20} from the recent past. Outside these regions, at higher latitudes, the boosting needed to represent the GS scenario of the LSG OGCM increases rapidly.

The boost $\Delta R_{20}^{Hol \rightarrow GS}$ does not however increase monotonically with latitude: it rises to a maximum around 60°S/70°N but then drops at the very poles. This is perhaps understandable since the greatest glacial boost will be needed when the local oceanic conditions in the GS scenario have changed most substantially from those seen in the Holocene/PD scenario. This occurs not at the poles themselves (where both the PD and GS scenarios have sea-ice) but rather slightly below the poles (where the GS scenario has sea-ice, but the PD does not). The extent of sea-ice in the different LSG OGCM scenarios can be found in Figures 3 and 10 of Butzin et al. (2005). At its greatest, around 60°S and 70°N, the GS scenario of the LSG OGCM suggests that glacial period $\Delta R_{20}(\theta)$ may be 1000 to 1500 ^{14}C yrs greater than in the recent past. If we fail to recognize the potential for such an increase in polar depletion when calibrating such high latitude samples against Marine20, then we may obtain calibrated ages that are ca. 1000 cal yrs too old.

An equivalent investigation of the changes required to a modern-day $\Delta R_{20}(\theta)$ to recreate the more extreme CS scenario of the LSG OGCM, while still using Marine20, can be found in the Supplementary Information C (Figures S3–S6). As for the GS scenario, the differences in modeled MRA between Marine20 and the CS scenario remain approximately constant over time, at least from 40,000–11,500 cal yr BP, at a given location. We can therefore obtain an

approximate CS scenario with Marine20 by applying a constant, latitude-dependent, boost $\Delta R_{20}^{\text{Hol} \rightarrow \text{CS}}$ to a modern-day ΔR_{20} estimate (Figure S5). The latitudinal $\Delta R_{20}^{\text{Hol} \rightarrow \text{CS}}$ shifts needed to be applied to recreate the CS scenario from Marine20 are, as expected, somewhat larger than the shifts required to recreate the GS scenario (Table A2, Appendix). A user wishing to be more cautious in calibration of samples during the glacial period may choose to select an upper bound for the polar ^{14}C depletion using this CS scenario.

3.2 Comparison with Independent Estimates of Surface MRA over Time

To provide an independent assessment of our proposed bracketing approach, we provide an illustration of the high- and low- depletion estimates of the overall MRA, $R_{20}^{\text{Location}}(\theta)$, that we would obtain from 40,000–0 cal yr BP at the location of deep-sea core MD04-2829 (59.0°N, 9.5°W; Skinner et al. 2019). This is a high-latitude site (59°N) within the Northern Atlantic where we might expect additional, localised, variations in $\Delta R_{20}(\theta)$ during the glacial period. We then compare our suggested bounding ^{14}C depletion scenarios against estimates of surface MRA obtained directly from this core's planktonic ^{14}C measurements. MD04-2829 has a calendar age-depth timescale based upon the alignment of changes in the abundance of planktonic foraminifer species *N. pachyderma* to the NGRIP $\delta^{18}\text{O}$ ice record (Svensson et al. 2008). Measurements of planktonic ^{14}C within the core can therefore be compared against IntCal20 to provide independent, and direct, estimates of the overall surface-atmospheric MRA.

Our bracketed estimates for $R_{20}^{\text{Location}}(\theta)$ are based on adjusting the global-scale $R_{20}^{\text{GlobalAv}}(\theta)$ of Marine20, just as would be implemented by a user of our approach. We first estimate a $\Delta R_{20}^{\text{Hol}}$ based upon the single most recent ^{14}C measurement within the MD04-2829 core. When combined with Marine20's $R_{20}^{\text{GlobalAv}}(\theta)$, this $\Delta R_{20}^{\text{Hol}}$ fixes the estimate for the overall MRA throughout the Holocene and determines the lower bound for the overall depletion in the glacial period. The resultant Holocene, and low-depletion glacial, estimate for $R_{20}^{\text{Location}}(\theta)$ is plotted in blue (with 1σ intervals). The location-specific upper bound for the glacial period is then calculated by applying the appropriate latitudinal shift $\Delta R_{20}^{\text{Hol} \rightarrow \text{GS}}$. In the case of MD04-2829 (at 59°N) this is 1000 ^{14}C yrs (see Table A2, Appendix). These shifted upper-bound glacial estimates are shown in red (with 1σ intervals).

We would hope that the directly observed MRA estimates obtained from planktonic ^{14}C measurements within the core (shown as black dots, with 1σ intervals) would lie between the two bounding (high- and low-) $R_{20}^{\text{Location}}(\theta)$ curves. Figure 5 shows this to generally be the case. We note that, during the Holocene, the blue $\Delta R_{20}^{\text{Hol}}$ -adjusted estimate appears a good fit. This suggests that Marine20's $R_{20}^{\text{GlobalAv}}(\theta)$ is capturing the main global-scale effects on the MRA; and that temporal variations in $\Delta R_{20}(\theta)$ are small during the Holocene (even at high latitudes). This supports our recommendation that, even at high-latitudes, users can continue using Marine20 (with a constant ΔR_{20}) during the Holocene.

Once we enter the glacial period however, we see that the observed MRAs in our high-latitude location vary significantly away from the low-depletion scenario. There are periods when $\Delta R_{20}(\theta)$ has clearly increased substantially in this polar marine location, and calibrating using the low-depletion scenario would not be appropriate. However, the directly observed estimates still lie within the upper- and lower-depletion curves, indicating that our bracketing approach is able to bound the variability in $\Delta R_{20}(\theta)$. As might be expected for a North Atlantic core such as MD04-2829, the regional $\Delta R_{20}(\theta)$ appears to increase during/around the Heinrich events and

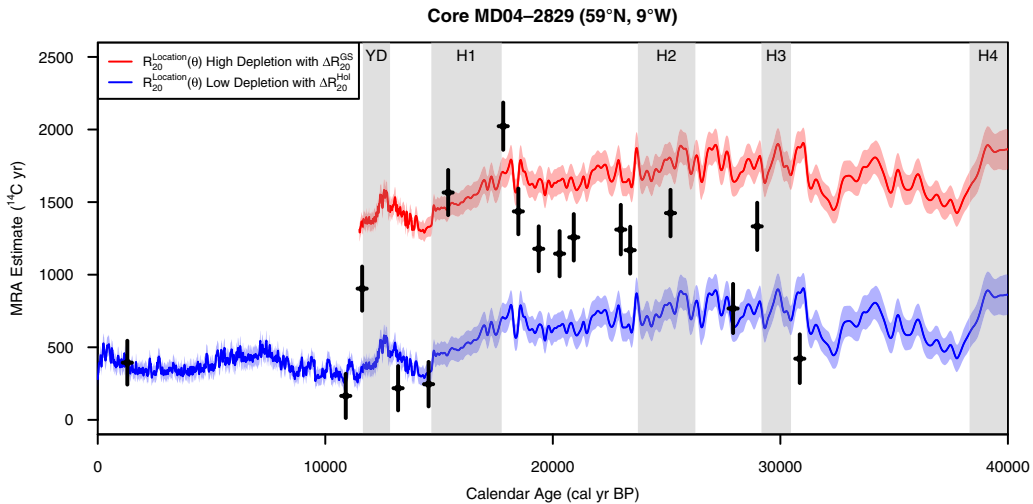


Figure 5 Plot of the upper and lower bounds on the overall MRA, $R_{20}^{Location}(\theta)$ obtained using our proposed bracketing approach compared against estimates of MRA calculated directly from planktic foraminifera (black dots) in the deep-sea core (MD04-2829, 59°N 9°W; Skinner et al. 2019). The high (red) and low (blue) depletion estimates shown are calculated by applying the appropriate latitudinal-shift to the global-scale $R_{20}^{GlobalAv}(\theta)$ of Marine20. Both the curves and the observations are shown with 1σ intervals. Heinrich events are overlain as shaded intervals.

around the LGM with the overall MRA moving towards its upper (red) limits, and then reduce away from these periods dropping back towards the lower (blue) limit.

4 POLAR CALIBRATION EXAMPLES (OFFSHORE VANCOUVER ISLAND 49°N, 127°W)

For our worked examples, we will consider the deep-sea core MD02-2496, sited offshore of Vancouver Island, Western Canada (Cosma et al. 2008; Taylor et al. 2014). This core is located at 48°58'47"N, 127°02'14"W and at 1243 m water depth. It contains a 38.38-m-long sequence of glaciomarine and hemipelagic sediments with 46 ^{14}C dates provided along the core. Two of these measurements lack depth information and so are not considered, and four have been removed as they are only reported as being greater than a certain ^{14}C yr BP. We will use the remaining 40 ^{14}C dates to illustrate the calibration of individual ^{14}C samples, and the creation of an age-depth model that combines all the data. OxCal code is provided in Supplementary Information E (single sample calibration) and F (age-depth model).

The location of core MD02-2496 has remained ice-sheet free, with the maximal extent of the Cordilleran ice sheet occurring around 18–19.5 cal kyr BP. However, we note that the proximity of this former ice sheet does complicate the issue of changes in $\Delta R(\theta)$ due to glacio-isostatic adjustments. Various sites along the British Columbia coast have had quite different sea level histories (Clague and James 2002). Such changes at a marine site may cause further changes to $\Delta R(\theta)$ over time.

For this site, we can estimate a modern-day value of ΔR_{20} based on samples from the recent past taken from <http://calib.org/marine/>, see Figure 6. The database contains eight samples from near the site of core MD02-2496. We discount the sample in David Channel (MapNo 949) as it relates to a deposit feeding organism (indicated by the red pushpin) and lies in a

channel rather than open ocean. Using the remaining seven samples, we obtain an estimate for a modern-day value of $\Delta R_{20} = 178 \pm 73$ ^{14}C yrs (1σ) using the online marine reservoir correction database tool (Reimer and Reimer 2001).

4.1 Calibration of Single ^{14}C Samples from Polar Regions

Suppose we wish to calibrate two individual ^{14}C samples taken from the deep-sea core site MD02-2496 at 49.0°N, 127.0°W:

1. *Holocene* Sample A (at depth 412 cm) with a ^{14}C age of 9215 ± 25 ^{14}C yrs BP (1σ)
2. *Glacial* Sample B (at depth 2057cm) with a ^{14}C age of 25190 ± 150 ^{14}C yrs BP (1σ)

Readers should note that these examples of individual calibration are intended as illustrations only. In practice, we would always suggest calibrating ^{14}C samples within a core together as part of an age-depth model rather than individually. By calibrating jointly, we can usually add strength to our calendar age estimation.

4.1.1 Calibration during the Holocene (9215 ± 25 ^{14}C yrs BP—Sample A)

Since the marine ^{14}C sample (sample A) that we wish to calibrate is from the Holocene, we do not need to incorporate a glacial increase in localized depletion. We can therefore calibrate the ^{14}C determination directly against Marine20 with the single value of ΔR_{20} calculated from the (recent past) samples shown in Figure 6. This calibration is shown in Figure 7 and provides a mean calibrated age estimate of 9570 cal yr BP, with a 95.4% confidence interval of [9340, 9840] cal yr BP.

Note that we can be confident that Sample A arises from the Holocene as the 95.4% calendar age range obtained under the calibration does not extend into the glacial. If the calendar age interval did extend beyond 11,500 cal yr BP, then we would advise that the dual approach of Section 4.1.2 is required.

4.1.2 Calibration during the Glacial (25190 ± 150 ^{14}C yrs BP—Sample B)

To calibrate a sample from the glacial period at the site of core MD02-2496, we must first calculate the increase, from the Holocene/recent-past ΔR_{20} , that is required to emulate the GS scenario of the LSG OGCM. At a latitude of 49°N, Figure 4 and Table A2 suggests an increase of 390 ^{14}C yrs is needed. We then calibrate against Marine20 under two different glacial scenarios. We hope these scenarios will bracket the ^{14}C depletion at the deep-sea site and time of the sample.

Calibrating in a low-depletion glacial scenario (oldest calendar age limit): To estimate the calendar age of the MD02-2496 ^{14}C determination ($25,190 \pm 150$ ^{14}C yrs BP) in a low-depletion glacial scenario, we calibrate against Marine20 using the level of regional ^{14}C depletion seen in the present day, i.e., $\Delta R_{MD02-2496}^{Hol} = \Delta R_{20} = 178 \pm 73$ ^{14}C yrs. This calibration still incorporates *global-scale* glacial conditions (e.g., the increase in ^{14}C concentrations, changes in CO_2 , and large-scale carbon cycle changes over the Holocene/pre-Holocene boundary that is included in Marine20) but does not incorporate the potential for regional sea-ice to temporally affect the site-specific $\Delta R_{20}(\theta)$.

Calibrating in a high-depletion glacial scenario (youngest calendar age limit): To calibrate in a high-depletion scenario that assumes regional/localized polar conditions similar to those

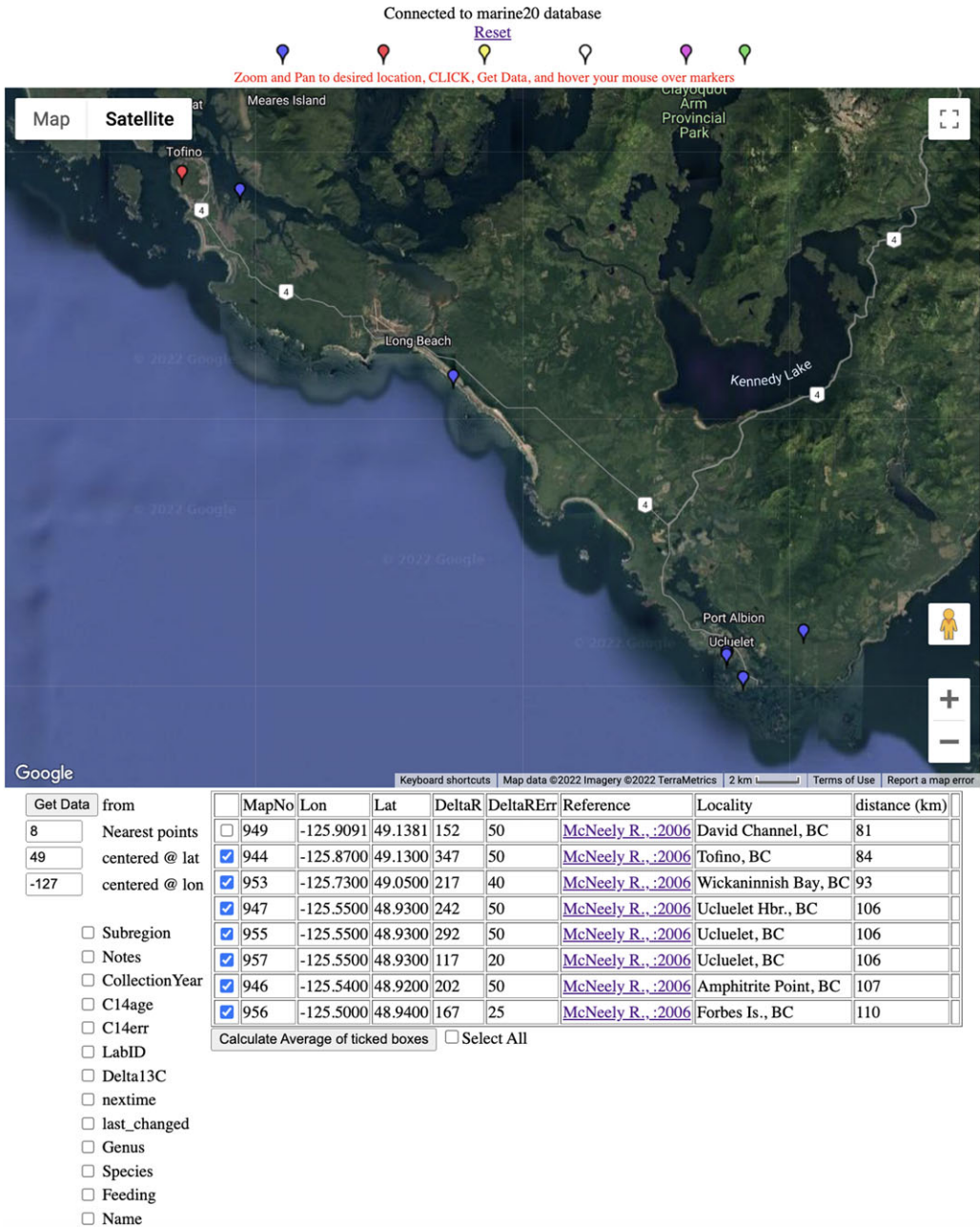


Figure 6 Location of ¹⁴C samples near sire MD02-2496 taken from the marine radiocarbon reservoir database (<http://calib.org/marine/>). We use the seven (modern-day) ticked samples to estimate a modern day ΔR_{20} for the site. We do not use MapNo 949 since this corresponds to a deposit-feeding organism (red pushpin) and lies in David Channel rather than the open ocean. Credit: Map data ©2021 GeoBasis-DE/BKG, Google Imagery ©2021 Terrametrics.

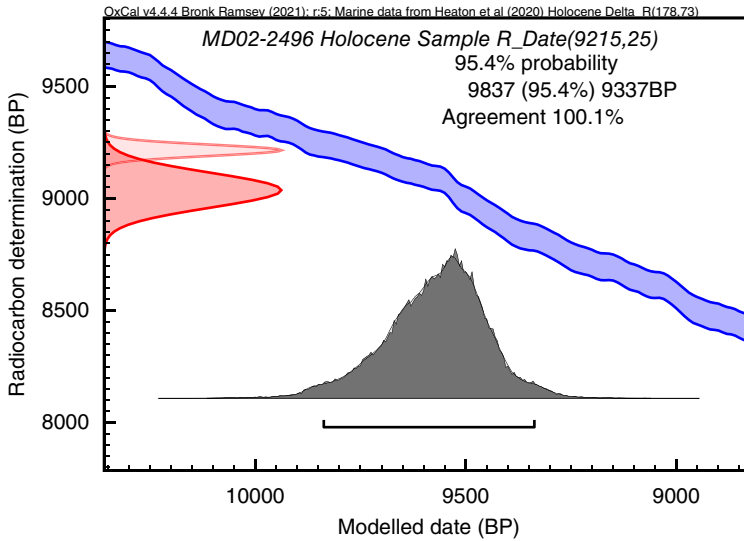


Figure 7 Calibration of marine sample A from the Holocene (9215 ± 25 ^{14}C yrs BP) taken from deep-sea core MD02-2496 (ca. 49.0°N , 127.0°W). We use a value of $\Delta R_{20} = 178 \pm 73$ ^{14}C yrs. Calibration is performed using OxCal v4.4.4 (Bronk Ramsey 2009) using the Marine20 calibration curve (Heaton et al. 2020). The Gaussian curves on the y-axis represent the raw ^{14}C -age (lighter) and the ΔR_{20} -adjusted ^{14}C -age (darker) of the marine sample. We calibrate the ΔR_{20} -adjusted ^{14}C -age against the Marine20 curve. The posterior calendar age estimate is shown along the x-axis. Note that, the OxCal calendar age scale runs from left (oldest) to right (youngest/more recent).

modeled in the GS scenario of the LSG OGCM, we add our latitudinal boost $\Delta R_{20}^{\text{Hol} \rightarrow \text{GS}}$ to the modern-day estimate of ΔR_{20} :

$$\Delta R_{\text{MD02-2496}}^{\text{GS}} = \Delta R_{\text{MD02-2496}}^{\text{Hol}} + \Delta R_{\text{MD02-2496}}^{\text{Hol} \rightarrow \text{GS}} = 178 + 390 = 568 \text{ }^{14}\text{C} \text{ yrs.}$$

We retain the same (1σ) uncertainty of ± 73 ^{14}C yrs taken from the value of ΔR_{20} . We then calibrate against Marine20 with this boosted $\Delta R_{\text{MD02-2496}}^{\text{GS}}$ estimate of regional depletion.

Obtaining bracketing calendar ages: The calendar age estimates obtained from calibrating the glacial sample ($25,190 \pm 150$ ^{14}C yrs BP) with the bracketing low- and high-depletion scenarios are shown in Figure 8 and Table 1. The overall calibrated age range covering both limiting depletion scenarios (running from the overall minimum calendar age to the maximum calendar age) is [27560, 28750] cal yr BP (Table 1). This combined interval aims to cover the maximum potential calendar age range for the ^{14}C sample. If we expect the true value of regional depletion $\Delta R(\theta)$ at the time the sample was exchanging with its environment to lie somewhere between the two extreme low- and high-depletion scenarios, the calendar age of the sample will also lie between the two scenario estimates. If no external knowledge is available regarding whether the low- or high- depletion glacial scenario is more appropriate for the sample, this extremely broad bracketing may be all we can provide. However, if independent information on the extent of sea-ice in the location is available, a calibration user may wish to make an argument that either the low- or high-depletion calibration scenarios (and hence calibrated ages) are more appropriate (or indeed argue for an intermediate level of depletion).

We stress that the combined (bracketed) interval of [27560, 28750] cal yr BP should have a coverage that is considerably greater than 95.4% (since it covers the two extremes). However,

Table 1 95.4% credible intervals for the calendar age of sample B (a glacial-period marine ^{14}C sample with a ^{14}C determination of $25,190 \pm 150$ ^{14}C yrs BP) from core MD02-2496 ($\sim 49^\circ\text{N}$) under a low- and high-depletion glacial scenario.

Scenario	95.4% calendar age interval (cal yr BP)
Low depletion $\Delta R_{MD02-2496}^{Hol} = 178 \pm 73$ ^{14}C yrs	[27870, 28750]
High depletion $\Delta R_{MD02-2496}^{GS} = 568 \pm 73$ ^{14}C yrs	[27560, 28410]
Combined scenario (age bracketing)	[27560, 28750]

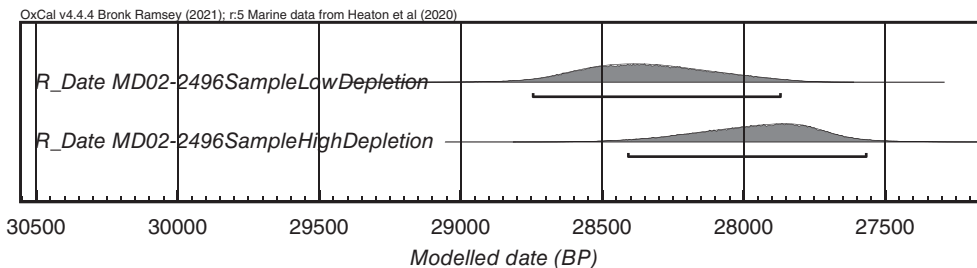


Figure 8 Calibration of glacial sample B with a ^{14}C determination of $25,190 \pm 150$ ^{14}C yrs BP from deep-sea core MD02-2496 (49°N 127°W). The top distribution shows the calibrated age under a low-depletion marine scenario (no additional changes in ^{14}C depletion over those seen in Equatorial waters). The bottom plot, the calibrated age under a high-depletion polar scenario (intended to represent conditions similar to the LGM). Note that the low-depletion glacial scenario (top) provides an older calendar age estimate—the OxCal calendar age scale runs from left (oldest) to right (youngest/more recent).

we do not provide any probability distribution on it, and no such distribution should be inferred as we expect that the true level of ^{14}C depletion may transition relatively rapidly between scenarios (spending less time at intermediate values) as sea-ice appears and disappears. Additionally, while in principle, there is no guarantee that the 95.4% quantiles for the calibrated age of a ^{14}C date decrease monotonically with increasing MRA/depletion levels (i.e., there might be an intermediate level of depletion which has 95.4% calendar age quantiles outside the range above) in practice, due to the smoothness of the current Marine20 estimate, there are no such cases pre-Holocene.

4.2 Calibrating Multiple ^{14}C Polar Determinations and Age Modeling

Polar ^{14}C calibration is also required when creating age-depth models for sediment cores based upon multiple ^{14}C determinations (e.g., McClymont et al. 2022; Taylor et al. 2014). For such age-depth models, ^{14}C calibration is typically done internally to the creation of the chronology. We recommend an analogous approach to that of Section 4.1. For those Holocene ^{14}C samples that are used to inform the overall chronology, we suggest a user apply a single ΔR_{20}^{Hol} ; while for older samples we suggest creating separate age-depth models under the low- and high-depletion scenarios. Then, when estimating the age at any specific depth, a user can read off the calendar age estimate for each age-depth model (low- and high-depletion) and use the same bracketing approach described in Section 4.1.2. Alternatively, they may wish to use independent palaeoclimatic/proxy evidence to support an age-depth model based on the level of ^{14}C depletion under one scenario (or to justify an intermediate level of depletion). As for the

calibration of single ¹⁴C samples, this can all be achieved within standard calibration software simply by adjusting, e.g., *DeltaR*, during age-depth model construction (see Supplementary Information F).

We consider an age-depth model fitted to the 40 ¹⁴C determinations in core MD02-2496 using OxCal's p-sequence (Bronk Ramsey 2008; Bronk Ramsey and Lee 2013). To create this model, we have averaged the two measurements (9215 ± 25 and $10,065 \pm 45$ ¹⁴C yrs BP) at 412cm into a single ¹⁴C date of 9415 ± 22 ¹⁴C yrs BP. For the low-depletion glacial scenario, we use a regional correction of $\Delta R_{MD02-2496}^{Hol} = 178 \pm 73$ ¹⁴C yrs as justified in the previous section; while for the high-depletion glacial scenario, we use a $\Delta R_{MD02-2496}^{GS} = 568 \pm 73$ ¹⁴C yrs. In this location, the transition between the Holocene and glacial corresponds to approximately 10,000 ¹⁴C yrs BP, i.e., a sample with a determination of 10,000 ¹⁴C yrs BP calibrates to being just older than 11,500 cal yr BP using a non-glacial $\Delta R_{MD02-2496}^{Hol} = 178 \pm 73$ ¹⁴C yrs. For both our high and low-depletion age-depth models, we therefore apply a Holocene value of $\Delta R(\theta)$ when constructing the age-depth model for all ¹⁴C samples at depths from 0–412 cm. Deeper in the core, we apply the appropriate high- and low-depletion glacial $\Delta R(\theta)$.

When fitting our OxCal p-sequence, we have selected a variable *k*, *P_Sequence*("",100,5,U(-2,2)), with core depths provided in m. There is one clear outlier with the sample at depth 5.52m ($14,025 \pm 50$ ¹⁴C yrs BP) being significantly older than the next five samples upcore at 5.92, 6.72, 7.57, 8.37, and 8.52m (ca. 13,300–13,900 ¹⁴C yrs BP). We have therefore used an outlier model with a prior probability of 0.05 of a sample being an outlier: *Outlier_Model*("General",T(5),U(0,4),"t").

The resultant models (with their uncertainty bands) are shown in Figure 9. The green age-depth model represents the chronology had core MD02-2496 been in a high-depletion $\Delta R_{MD02-2496}^{GS}$ polar scenario throughout the glacial period before shifting to $\Delta R_{MD02-2496}^{Hol}$ in the Holocene. In the blue age-depth model, $\Delta R(\theta) = \Delta R_{MD02-2496}^{Hol}$ throughout. This represents the chronology if the climate at site MD02-2496 had followed a low-depletion polar scenario throughout the glacial where no additional regional changes in oceanic ¹⁴C depletion were seen beyond those large-scale effects captured in Marine20.

If we are interested in the calendar age of a hypothetical event at depth of 15.2m in the core (as illustrated in Figure 9), then we can obtain calendar age estimates from the separate age-depth models under the low- and high-depletion glacial polar scenarios. These calendar ages are shown in Table 2. Again, these can be combined by selecting the most extreme calendar ages to create a wide age-bracketing that hopefully includes the true calendar age.

We note that it is possible that the true $\Delta R(\theta)$ flips between the high- and low-depletion polar glacial scenarios over time throughout the core as we move from stadials to interstadials. Our suggested bracketing age-depth models assume a constant $\Delta R(\theta)$ depletion scenario (either high or low). Such scenario flips could change the age-depth model substantially. However, preliminary testing suggests that even with changes from high- to low-depletion within the core, the calendar ages from the fixed, bounding, glacial scenarios bracket the calendar ages of the scenario-changing model at any given depth. Users of age-depth models may also wish to place a uniform prior on their estimate of $\Delta R(\theta)$ with upper- and lower-bounds taken from the low- and high-depletion scenarios. Such a model would provide a single age-depth model. However, if the climate flips rapidly between climate scenarios, with the appropriate $\Delta R(\theta)$ also flipping between its upper and lower limits, this approach may give over-confident estimates.

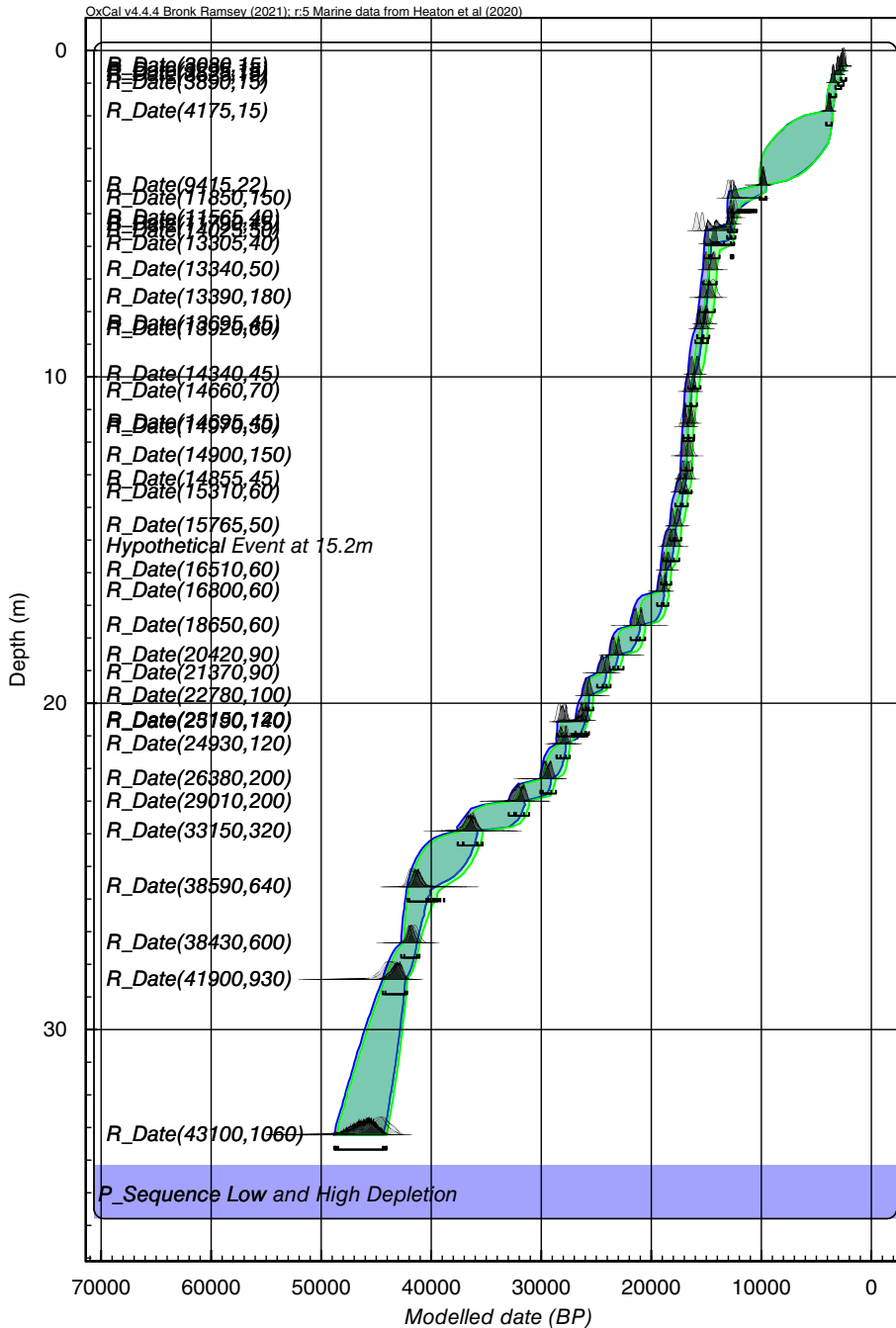


Figure 9 Age-depth models of deep-sea core MD02-2496 (49°N 127°W) under a low (blue) and high (green) depletion polar scenario using an OxCal p-sequence (with a variable k and general outlier model). Changes in depletion can be achieved by modification of DeltaR within OxCal's p-sequence model. Core depths are given in m. We consider the age of a hypothetical event at 15.2 m within the core. Again, the OxCal calendar age scale runs from left (oldest) to right (youngest/more recent).

Table 2 Calendar age estimates of the MD02-2496 (49°N) sediment core at a depth of 15.2 m based on OxCal's p-sequence age-depth modeling (with a variable k and general outlier model) under the low- and high-depletion polar scenarios.

Scenario:	95.4% calendar age interval (cal yr BP)
Calendar age at depth of 15.2 m in MD02-2496	
Low depletion $\Delta R_{MD02-2496}^{Hol} = 178 \pm 73$ ¹⁴ C yrs	[17950, 18950]
High depletion $\Delta R_{MD02-2496}^{GS} = 568 \pm 73$ ¹⁴ C yrs	[17460, 18550]
Combined scenario (bracketing)	[17460, 18950]

4.3 Incorporating Paleoclimatic and Proxy Evidence on the Sea-Ice Extent into Calibration

We recommend that all those calibrating glacial period ¹⁴C samples from polar regions present the results from both bracketing scenarios, with the belief that the true calendar ages should lie between the values obtained under the two limiting scenarios. However, we recognize that some users may have expert knowledge from independent palaeoclimatic/proxy evidence as to which scenario is more appropriate. Such users might therefore, quite reasonably, wish to argue one option is more plausible than the other; or indeed they may believe that an intermediate ¹⁴C depletion scenario (which would result in intermediate calendar ages) is most suitable. We leave such interpretation up to the individual expert and would encourage them to do so if it is felt appropriate, provided their reasoning is fully documented.

Further into the future, it may be possible to determine more precise $\Delta R(\theta)$ regional adjustments in polar regions using paleoclimatic and proxy evidence to infer the extent of sea-ice. Such proxy information might allow one to scale, for any individual ¹⁴C sample, the $\Delta R(\theta)$ between the present-day ΔR_{20} value and that representing the GS/CS values of the LSG OGCM. If such a procedure was shown to improve our estimation of polar $\Delta R(\theta)$, then it would also provide more precise calendar dating when calibrating polar ¹⁴C samples. Reconstructing sea-ice variation is possible but challenging. Several proxies have been proposed. These include micropaleontological transfer functions based on diatoms (e.g., Gersonde et al. 2005) and dinocysts (de Vernal et al. 2001); molecular abundance of a particular hydrocarbon (IP25) synthesized by diatoms living at the bottom of sea-ice (Belt and Müller 2013); and stomach-oil deposits from snow petrels (McClymont et al. 2022; Thatje et al. 2008). Several authors have used these proxies to show systematic changes of sea-ice that are linked to abrupt climate changes (Hoff et al. 2016; Méheust et al. 2018; Stein et al. 2017). To investigate whether such a sliding, sea-ice proxy-informed, $\Delta R(\theta)$ correction improves calendar dating would require suitable independent testing: either by comparing the resultant core chronology against absolute chronologies; or with downcore evidence of local MRA changes (e.g., using tephra). Such work goes beyond that possible here but would be a valuable further avenue of study.

5 CONCLUSIONS

Estimating the evolution of surface-ocean ¹⁴C levels in polar regions from 55,000–0 cal yr BP, and consequently calibrating marine ¹⁴C samples from these high-latitude region, is highly challenging. All of the MarineXX radiocarbon age calibration curves (Marine20 and all earlier products) only aim to represent *global-scale* changes in oceanic ¹⁴C levels (Heaton et al. 2020, 2022). The recent Marine20 curve incorporates large-scale changes in paleoclimate and the carbon cycle which occurred during the glacial: most notably in CO₂ (Köhler et al. 2017),

atmospheric ^{14}C (Reimer et al. 2020), wind speed (Kageyama et al. 2021; Kohfeld et al. 2013; Petit et al. 1990) and AMOC (Böhm et al. 2015; Henry et al. 2016; Oka et al. 2021). However, in polar regions, we expect that during glacial periods there may have been substantial further, more localized, changes in the level of oceanic ^{14}C depletion. This additional polar variation is due, in particular, to increases in the volume and density of sea-ice at high-latitudes during these periods (Butzin et al. 2005, 2017, 2020). These temporal variations in the MRA at high-latitudes during the glacial period are not represented in the *global-scale* MarineXX curves, and so must be modeled through $\Delta R(\theta)$.

When calibrating marine ^{14}C samples against Marine20, or any MarineXX curve, using an appropriate value of $\Delta R(\theta)$ is critical. Typically, we are only able to estimate a modern-day value for $\Delta R(\theta)$ using ^{14}C samples from the recent past. This (modern-day) estimate of ΔR is unlikely to be suitable for application when calibrating high-latitude (outside *ca.* 40°S–40°N) marine ^{14}C samples from the glacial period against Marine20, or any MarineXX curve. We expect that, for polar oceans, due to the presence of regional sea-ice, the value of $\Delta R(\theta)$ may have been substantially greater during the glacial period than those values seen during the non-glacial recent past. Under some modeled climate scenarios, the increase in the value of $\Delta R(\theta)$ in polar regions could extend up to *ca.* 1500 ^{14}C yrs (Butzin et al. 2020).

If we calibrate a polar marine ^{14}C sample from the glacial period using a modern-day estimate of $\Delta R(\theta)$, without recognizing the potential for this $\Delta R(\theta)$ to increase in glacial conditions, we are likely to obtain a calibrated age that is biased (older than the true calendar age) and over precise. Current proxy records are not sufficiently reliable to reconstruct the climatic conditions at high-latitudes (including the extent of sea-ice, ocean ventilation and wind strengths) during the glacials. Due to this considerable uncertainty in polar paleoclimate, it is not possible to accurately or precisely model $\Delta R(\theta)$ and generate polar radiocarbon age calibration curves. The LSG OGCM model does permit modeling of surface open-ocean ^{14}C levels in polar regions under fixed climate scenarios (Butzin et al. 2020). However, direct use of these LSG OGCM estimates for calibration is not trivial.

We propose that those wishing to calibrate high-latitude (outside *ca.* 40°S–40°N) marine ^{14}C samples may continue to use the Marine20 curves but with a simple and approximate adjustment to the value of $\Delta R(\theta)$ dependent upon the calendar age and latitude of the sample. We suggest that those calibrating polar marine ^{14}C samples from the Holocene proceed as they traditionally have done, by estimating a regional ΔR_{20} based on samples from the recent past, and then assuming this ΔR_{20} value remains applicable for their undated sample.

For those wishing to estimate the calendar ages of polar marine ^{14}C samples from glacial periods we suggest using two bracketing surface-ocean ^{14}C depletion scenarios. The first (low-depletion) scenario assumes that there have been no regional changes in polar $\Delta R(\theta)$ over time. The calendar age of the ^{14}C sample under this scenario can be obtained by calibrating against Marine20 using an estimate of $\Delta R_{20}^{\text{Hol}}$ based on samples from the recent past in the location of interest. The second (high-depletion) scenario aims to represent the GS glacial scenario of the LSG OGCM (which includes considerable high-latitude sea-ice). This scenario can be approximated with Marine20 simply by increasing the (recent-past) estimate of $\Delta R_{20}^{\text{Hol}}$ by a latitude dependent constant $\Delta R^{\text{Hol} \rightarrow \text{GS}}$. This boost to the localized ^{14}C depletion aims to provide an upper limit on the potential level of additional regional polar ^{14}C depletion in the glacial.

We hope that the calibrated age estimates obtained using Marine20 under these two polar glacial depletion scenarios will bracket the true calendar age of the ¹⁴C sample. The low-depletion scenario will provide an upper calendar age limit, the high-depletion a lower calendar age limit. If no external information is available regarding which depletion scenario is more appropriate, then one may only be able to infer that the true calendar age lies between these upper and lower limits. This range will typically be wide. However, if paleoclimatic proxies are available, for example on the extent of sea-ice, then a user may be able to infer which scenario is more appropriate. While we recommend that the calibrated dates under both high- and low-depletion scenarios are always shown so that a reader can understand the likely maximum range of calibrated dates, a user with independent information on the most suitable depletion scenario may focus their later interpretation on that provided their reasoning is documented.

As knowledge increases, we expect that polar-specific calibration curves will become available. Such advances could be obtained via improved modeling, although this will require significantly improved understanding of paleoceanographic proxy information to better reconstruct past polar climate. Alternatively, polar marine curves could be generated by collecting ¹⁴C samples in the relevant ocean locations, if it is possible to date these samples via alternative techniques.

ACKNOWLEDGMENTS

TJH is supported by the BA/Leverhulme (SRG22/220289), NERC (NE/X009815/1), and a Leverhulme Trust Fellowship RF-2019-140/9. E. Bard and M. Butzin are funded by the joint ANR-DFG project MARCARA. P. Köhler and also M. Butzin were supported by the German Federal Ministry of Education and Research (BMBF), as Research for Sustainability initiative (FONA); www.fona.de through the PalMod project (grant numbers: 01LP1505B, 01LP1919A).

SUPPLEMENTARY MATERIAL

To view supplementary material for this article, please visit <https://doi.org/10.1017/RDC.2023.42>

REFERENCES

- Bard E. 1988. Correction of accelerator mass spectrometry ¹⁴C ages measured in planktonic foraminifera: paleoceanographic implications. *Paleoceanography* 3(6):635–645. doi: [10.1029/PA003i006p00635](https://doi.org/10.1029/PA003i006p00635)
- Belt ST, Müller J. 2013. The Arctic sea ice biomarker IP25: a review of current understanding, recommendations for future research and applications in palaeo sea ice reconstructions. *Quaternary Science Reviews* 79:9–25. doi: [10.1016/j.quascirev.2012.12.001](https://doi.org/10.1016/j.quascirev.2012.12.001)
- Böhm E, Lippold J, Gutjahr M, Frank M, Blaser P, Antz B, Fohlmeister J, Frank N, Andersen MB, Deininger M. 2015. Strong and deep Atlantic meridional overturning circulation during the last glacial cycle. *Nature* 517(7532):73–76. doi: [10.1038/nature14059](https://doi.org/10.1038/nature14059)
- Bronk Ramsey C. 2008. Deposition models for chronological records. *Quaternary Science Reviews* 27(1):42–60. doi: [10.1016/j.quascirev.2007.01.019](https://doi.org/10.1016/j.quascirev.2007.01.019)
- Bronk Ramsey C. 2009. Bayesian analysis of radiocarbon dates. *Radiocarbon* 51(1):337–360. doi: [10.1017/S0033822200033865](https://doi.org/10.1017/S0033822200033865)
- Bronk Ramsey C, Lee S. 2013. Recent and planned developments of the program OxCal. *Radiocarbon* 55(2):720–730. doi: [10.1017/S0033822200057878](https://doi.org/10.1017/S0033822200057878)
- Butzin M, Heaton TJ, Köhler P, Lohmann G. 2020. A short note on marine reservoir age simulations used in IntCal20. *Radiocarbon* 62(4):865–871. doi: [10.1017/RDC.2020.9](https://doi.org/10.1017/RDC.2020.9)
- Butzin M, Köhler P, Lohmann G. 2017. Marine radiocarbon reservoir age simulations for the past

- 50,000 years. *Geophysical Research Letters* 44(16):8473–8480. doi: [10.1002/2017GL074688](https://doi.org/10.1002/2017GL074688)
- Butzin M, Prange M, Lohmann G. 2005. Radiocarbon simulations for the glacial ocean: the effects of wind stress, Southern Ocean sea ice and Heinrich events. *Earth and Planetary Science Letters* 235(1–2):45–61. doi: [10.1016/j.epsl.2005.03.003](https://doi.org/10.1016/j.epsl.2005.03.003)
- Clague JJ, James TS. 2002. History and isostatic effects of the last ice sheet in southern British Columbia. *Quaternary Science Reviews* 21(1):71–87. doi: [10.1016/S0277-3791\(01\)00070-1](https://doi.org/10.1016/S0277-3791(01)00070-1)
- Cosma TN, Hendy IL, Chang AS. 2008. Chronological constraints on Cordilleran Ice Sheet glaciomarine sedimentation from core MD02-2496 off Vancouver Island (western Canada). *Quaternary Science Reviews* 27(9):941–955. doi: [10.1016/j.quascirev.2008.01.013](https://doi.org/10.1016/j.quascirev.2008.01.013)
- De Boer AM, Nof D. 2004. The Bering Strait's grip on the northern hemisphere climate. *Deep Sea Research Part I: Oceanographic Research Papers* 51(10):1347–1366. doi: [10.1016/j.dsr.2004.05.003](https://doi.org/10.1016/j.dsr.2004.05.003)
- de Vernal A, Henry M, Matthiessen J, Mudie PJ, Rochon A, Boessenkool KP, Eynaud F, Grösfjeld K, Guiot J, Hamel D, et al. 2001. Dinoflagellate cyst assemblages as tracers of sea-surface conditions in the northern North Atlantic, Arctic and sub-Arctic seas: the new 'n = 677' data base and its application for quantitative palaeoceanographic reconstruction. *Journal of Quaternary Science* 16(7):681–698. doi: [10.1002/jqs.659](https://doi.org/10.1002/jqs.659)
- Gersonde R, Crosta X, Abelmann A, Armand L. 2005. Sea-surface temperature and sea ice distribution of the Southern Ocean at the EPILOG Last Glacial Maximum—a circum-Antarctic view based on siliceous microfossil records. *Quaternary Science Reviews* 24(7):869–896. doi: [10.1016/j.quascirev.2004.07.015](https://doi.org/10.1016/j.quascirev.2004.07.015)
- Heaton TJ, Bard E, Bronk Ramsey C, Butzin M, Hatte C, Hughen KA, Köhler P, Reimer PJ. 2022. A response to community questions on the Marine20 Radiocarbon age calibration curve: marine reservoir ages and the calibration of ^{14}C samples from the oceans. *Radiocarbon* 65(1):247–273. doi: [10.1017/RDC.2022.66](https://doi.org/10.1017/RDC.2022.66)
- Heaton TJ, Köhler P, Butzin M, Bard E, Reimer RW, Austin WEN, Bronk Ramsey C, Grootes PM, Hughen KA, Kromer B, et al. 2020. Marine20—the marine radiocarbon age calibration curve (0–55,000 cal BP). *Radiocarbon* 62(4):779–820. doi: [10.1017/RDC.2020.68](https://doi.org/10.1017/RDC.2020.68)
- Henry LG, McManus JF, Curry WB, Roberts NL, Piotrowski AM, Keigwin LD. 2016. North Atlantic ocean circulation and abrupt climate change during the last glaciation. *Science* 353(6298):470–474. doi: [10.1126/science.aaf5529](https://doi.org/10.1126/science.aaf5529)
- Hodell DA, Venz KA, Charles CD, Ninnemann US. 2003. Pleistocene vertical carbon isotope and carbonate gradients in the South Atlantic sector of the Southern Ocean. *Geochemistry, Geophysics, Geosystems* 4(1):1–19. doi: [10.1029/2002GC000367](https://doi.org/10.1029/2002GC000367)
- Hoff U, Rasmussen TL, Stein R, Ezat MM, Fahl K. 2016. Sea ice and millennial-scale climate variability in the Nordic seas 90 kyr ago to present. *Nature Communications*, 7(1):12247. doi: [10.1038/ncomms12247](https://doi.org/10.1038/ncomms12247)
- Hughen KA, Baillie MGL, Bard E, Beck JW, Bertrand CJH, Blackwell PG, Buck CE, Burr GS, Cutler KB, Damon PE, et al. 2004. Marine04 marine radiocarbon age calibration, 0–26 cal kyr BP. *Radiocarbon* 46(3):1059–1086. doi: [10.1017/S0033822200033002](https://doi.org/10.1017/S0033822200033002)
- Jakobsson M, Pearce C, Cronin TM, Backman J, Anderson LG, Barrientos N, Björk G, Coxall H, de Boer A, Mayer LA, et al. 2017. Post-glacial flooding of the Bering Land Bridge dated to 11 cal ka BP based on new geophysical and sediment records. *Clim. Past* 13(8):991–1005. doi: [10.5194/cp-13-991-2017](https://doi.org/10.5194/cp-13-991-2017)
- Kageyama M, Harrison SP, Kapsch M-L, Lofverstrom M, Lora JM, Mikolajewicz U, Sherriff-Tadano S, Vadsaria T, Abe-Ouchi A, Bouttes N, et al. 2021. The PMIP4 Last Glacial Maximum experiments: preliminary results and comparison with the PMIP3 simulations. *Clim. Past* 17(3):1065–1089. doi: [10.5194/cp-17-1065-2021](https://doi.org/10.5194/cp-17-1065-2021)
- Key RM. 2001. Radiocarbon. In: *Encyclopedia of ocean sciences* Academic Press. p. 2338–2353. doi: [10.1006/rwos.2001.0162](https://doi.org/10.1006/rwos.2001.0162)
- Key RM, Kozyr A, Sabine CL, Lee K, Wanninkhof R, Bullister JL, Feely RA, Millero FJ, Mordy C, Peng T-H. 2004. A global ocean carbon climatology: Results from Global Data Analysis Project (GLODAP). *Global Biogeochemical Cycles* 18(4):GB4031. doi: [10.1029/2004GB002247](https://doi.org/10.1029/2004GB002247)
- Knudson KP, Ravelo AC. 2015. North Pacific Intermediate Water circulation enhanced by the closure of the Bering Strait. *Paleoceanography* 30(10):1287–1304. doi: [10.1002/2015PA002840](https://doi.org/10.1002/2015PA002840)
- Kohfeld KE, Graham RM, de Boer AM, Sime LC, Wolff EW, Le Quééré C, Bopp L. 2013. Southern Hemisphere westerly wind changes during the Last Glacial Maximum: paleo-data synthesis. *Quaternary Science Reviews* 68:76–95. doi: [10.1016/j.quascirev.2013.01.017](https://doi.org/10.1016/j.quascirev.2013.01.017)
- Köhler P, Fischer H, Schmitt J. 2010. Atmospheric $\delta^{13}\text{C}$ and its relation to $p\text{CO}_2$ and deep ocean $\delta^{13}\text{C}$ during the late Pleistocene. *Paleoceanography* 25(1):PA1213. doi: [10.1029/2008PA001703](https://doi.org/10.1029/2008PA001703)
- Köhler P, Muscheler R, Fischer H. 2006. A model-based interpretation of low-frequency changes in the carbon cycle during the last 120,000 years and its implications for the reconstruction of atmospheric $\Delta^{14}\text{C}$. *Geochemistry, Geophysics, Geosystems* 7:Q11N06. doi: [10.1029/2005GC001228](https://doi.org/10.1029/2005GC001228)
- Köhler P, Nehrbass-Ahles C, Schmitt J, Stocker TF, Fischer H. 2017. A 156 kyr smoothed history of the atmospheric greenhouse gases CO_2 , CH_4 , and N_2O and their radiative forcing. *Earth System*

- Science Data 9(1):363–387. doi: [10.5194/essd-9-363-2017](https://doi.org/10.5194/essd-9-363-2017)
- Lambeck K, Rouby H, Purcell A, Sun Y, Sambridge M. 2014. Sea level and global ice volumes from the Last Glacial Maximum to the Holocene. *Proceedings of the National Academy of Sciences*, 111(43):15296–15303. doi: [10.1073/pnas.1411762111](https://doi.org/10.1073/pnas.1411762111)
- Levin I, Heshaimer V. 2000. Radiocarbon – a unique tracer of global carbon cycle dynamics. *Radiocarbon* 42(1):69–80. doi: [10.1017/S0033822200053066](https://doi.org/10.1017/S0033822200053066)
- McClymont EL, Bentley MJ, Hodgson DA, Spencer-Jones CL, Wardley T, West D, Croudace JW, Berg S, Gröcke DR, Kuhn G, Jamieson SSR, Sime L, Phillips RA. 2022. Summer sea-ice variability on the Antarctic margin during the last glacial period reconstructed from snow petrel (*Pagodroma nivea*) stomach-oil deposits. *Clim. Past* 18(2):381–403. doi: [10.5194/cp-18-381-2022](https://doi.org/10.5194/cp-18-381-2022)
- McGee D, Broecker WS, Winckler, G. 2010. Gustiness: the driver of glacial dustiness? *Quaternary Science Reviews* 29(17):2340–2350. doi: [10.1016/j.quascirev.2010.06.009](https://doi.org/10.1016/j.quascirev.2010.06.009)
- Méheust M, Stein R, Fahl K, Gersonde R. 2018. Sea-ice variability in the subarctic North Pacific and adjacent Bering Sea during the past 25 ka: new insights from IP25 and Uk'37 proxy records. *Arktos* 4(1):1–19. doi: [10.1007/s41063-018-0043-1](https://doi.org/10.1007/s41063-018-0043-1)
- Oka A, Abe-Ouchi A, Sherriff-Tadano S, Yokoyama Y, Kawamura K, Hasumi H. 2021. Glacial mode shift of the Atlantic meridional overturning circulation by warming over the Southern Ocean. *Communications Earth & Environment* 2(1):169. doi: [10.1038/s43247-021-00226-3](https://doi.org/10.1038/s43247-021-00226-3)
- Petit JR, Mournier L, Jouzel J, Korotkevich YS, Kotlyakov VI, Lorius C. 1990. Palaeoclimatological and chronological implications of the Vostok core dust record. *Nature* 343(6253):56–58. doi: [10.1038/343056a0](https://doi.org/10.1038/343056a0)
- Reimer PJ, Austin WEN, Bard E, Bayliss A, Blackwell PG, Ramsey CB, Butzin M, Cheng H, Edwards RL, Friedrich M, et al. 2020. The IntCal20 Northern Hemisphere radiocarbon age calibration curve (0–55 cal kBP). *Radiocarbon* 62(4):725–757. doi: [10.1017/RDC.2020.41](https://doi.org/10.1017/RDC.2020.41)
- Reimer PJ, Baillie MGL, Bard E, Bayliss A, Beck JW, Blackwell PG, Bronk Ramsey C, Buck CE, Burr GS, Edwards RL, et al. 2009. IntCal09 and Marine09 radiocarbon age calibration curves, 0–50,000 years cal BP. *Radiocarbon* 51(4):1111–1150. doi: [10.1017/s0033822200034202](https://doi.org/10.1017/s0033822200034202)
- Reimer PJ, Bard E, Bayliss A, Beck JW, Blackwell PG, Bronk Ramsey C, Buck C, Cheng H, Edwards RL, Friedrich M, et al. 2013. IntCal13 and Marine13 radiocarbon age calibration curves 0–50,000 years cal BP. *Radiocarbon* 55(4):1869–1887. doi: [10.2458/azu_js_rc.55.16947](https://doi.org/10.2458/azu_js_rc.55.16947)
- Reimer PJ, Reimer RW. 2001. A marine reservoir correction database and on-line interface. *Radiocarbon* 43(2A):461–463. doi: [10.1017/S0033822200038339](https://doi.org/10.1017/S0033822200038339)
- Skinner LC, Muschitiello F, Scrivner AE. 2019. Marine reservoir age variability over the last deglaciation: implications for marine carbon cycling and prospects for regional radiocarbon calibrations. *Paleoceanography and Paleoclimatology* 34(11):1807–1815. doi: [10.1029/2019PA003667](https://doi.org/10.1029/2019PA003667)
- Stein R, Fahl K, Gierz P, Niessen F, Lohmann G. 2017. Arctic Ocean sea ice cover during the penultimate glacial and the last interglacial. *Nature Communications* 8(1):373. doi: [10.1038/s41467-017-00552-1](https://doi.org/10.1038/s41467-017-00552-1)
- Stuiver M, Braziunas TF. 1993. Modeling atmospheric ¹⁴C influences and ¹⁴C ages of marine samples to 10,000 BC. *Radiocarbon* 35(1):137–189. doi: [10.1017/S0033822200013874](https://doi.org/10.1017/S0033822200013874)
- Stuiver M, Pearson GW, Braziunas T. 1986. Radiocarbon age calibration of marine samples back to 9000 cal yr BP. *Radiocarbon* 28(2B):980–1021. doi: [10.1017/S0033822200060264](https://doi.org/10.1017/S0033822200060264)
- Stuiver M, Reimer PJ, Bard E, Beck JW, Burr GS, Hughen KA, Kromer B, McCormac G, van der Plicht J, Spurk M. 1998. INTCAL98 Radiocarbon Age Calibration, 24,000–0 cal BP. *Radiocarbon* 40(3):1041–1083. doi: [10.1017/S0033822200019123](https://doi.org/10.1017/S0033822200019123)
- Svensson A, Andersen KK, Bigler M, Clausen HB, Dahl-Jensen D, Davies SM, Johnsen SJ, Muscheler R, Parrenin F, Rasmussen SO, Röthlisberger R, Seierstad I, Steffensen JP, Vinther BM. 2008. A 60 000 year Greenland stratigraphic ice core chronology. *Clim. Past* 4(1):47–57. doi: [10.5194/cp-4-47-2008](https://doi.org/10.5194/cp-4-47-2008)
- Taylor MA, Hendy IL, Pak DK. 2014. Deglacial ocean warming and marine margin retreat of the Cordilleran Ice Sheet in the North Pacific Ocean. *Earth and Planetary Science Letters* 403:89–98. doi: [10.1016/j.epsl.2014.06.026](https://doi.org/10.1016/j.epsl.2014.06.026)
- Thatje S, Hillenbrand C-D, Mackensen A, Larter R. 2008. Life hung by a thread: endurance of Antarctic fauna in glacial periods. *Ecology* 89(3):682–692. <http://www.jstor.org/stable/27651591>
- Toggweiler JR, Druffel ERM, Key RM, Galbraith ED. 2019. Upwelling in the ocean basins north of the ACC: 1. On the upwelling exposed by the surface distribution of $\Delta^{14}\text{C}$. *Journal of Geophysical Research: Oceans* 124(4):2591–2608. doi: [10.1029/2018JC014794](https://doi.org/10.1029/2018JC014794)
- Völker C, Köhler P. 2013. Responses of ocean circulation and carbon cycle to changes in the position of the Southern Hemisphere westerlies at Last Glacial Maximum. *Paleoceanography* 28(4):726–739. doi: [10.1002/2013PA002556](https://doi.org/10.1002/2013PA002556)

Appendix A

Table A1 Key notation used to define various components of marine reservoir age.

$R^{Location}(\theta)$	The overall MRA (depletion between atmosphere and surface-ocean) at a specific location and calendar age θ : $R^{Location}(\theta) = R^{GlobalAv}(\theta) + \Delta R^{Location}(\theta)$
$R_{20}^{GlobalAv}(\theta)$	The component of the overall MRA that incorporates the global-scale effects (i.e., the variability in MRA which is shared between locations). This is modeled by the Marine20 curve.
$\Delta R_{20}^{Location}(\theta)$	The localized component of the overall MRA (i.e., the variability which is not captured by the global-scale $R_{20}^{GlobalAv}(\theta)$ component). The value of $\Delta R_{20}^{Location}(\theta)$ could be influenced by factors including depth of ocean, regional winds, coastal upwelling, . . .
$\Delta R_{20} / \Delta R_{20}^{Hol}$	A present-day estimate of $\Delta R_{20}^{Location}(\theta)$ based upon samples from the recent past (or Holocene respectively). Typically, we calibrate using the simplification that $\Delta R_{20}^{Location}(\theta) = \Delta R_{20}$ throughout the Holocene.
$\Delta R_{20}^{GS/CS}$	The value of $\Delta R_{20}^{Location}(\theta)$ that would approximately correspond to the level of surface-ocean ^{14}C depletion seen under the GS (or CS respectively) modeling scenario of the LSG OGCM during the glacial
$\Delta R_{20}^{Hol \rightarrow GS/CS}$	The boost to a modern-day (Holocene) based estimate of ΔR_{20} needed to recreate the GS (or CS respectively) modeling scenario of the LSG OGCM during the glacial, $\Delta R_{20}^{Hol \rightarrow GS/CS} = \Delta R_{20}^{GS/CS} - \Delta R_{20}^{Hol}$

Table A2 Estimates of the latitudinal increases $\Delta R^{Hol \rightarrow GS}$ (and $\Delta R^{Hol \rightarrow CS}$) to be applied to modern-day ΔR_{20} if we wish to recreate the GS (and CS) scenarios of the LSG OGCM in the glacial periods while still using the Marine20 curve. Those values highlighted in gold (outside ~40°S–40°N) have shifts which fall outside the mean $\pm 2\sigma$ uncertainty on the value of $R_{20}^{GlobalAv}(\theta)$ that is already incorporated into the global-scale Marine20 curve. We suggest that, when calibrating glacial-period ¹⁴C samples from marine locations at these higher (gold) latitudes, users should employ our bracketing approach to allow for low- and high-depletion glacial polar scenarios. At lower latitudes (highlighted in green) we cautiously suggest that users do not need to consider such bracketing as the increase to recreate the GS (or CS) scenarios falls within the existing uncertainty on the Marine20 curve. Users with sites at latitudes not specified above should interpolate (although remain aware that all these estimates are, by design, coarse and hence do not need to focus on over-precision).

Latitude °N	GS Scenario	CS Scenario	Latitude °S	GS Scenario	CS Scenario
88.75	730	1060	88.75	NA	NA
86.25	720	1060	86.25	NA	NA
83.75	730	1060	83.75	NA	NA
81.25	740	1050	81.25	NA	NA
78.75	790	1100	78.75	NA	NA
76.25	870	1160	76.25	NA	NA
73.75	960	1180	73.75	460	660
71.25	1110	1220	71.25	470	680
68.75	1400	1340	68.75	580	790
66.25	1370	1320	66.25	720	940
63.75	1190	1340	63.75	940	1160
61.25	1100	1390	61.25	1090	1290
58.75	990	1380	58.75	1090	1300
56.25	660	1070	56.25	1000	1190
53.75	540	920	53.75	880	1060
51.25	450	810	51.25	740	920
48.75	390	740	48.75	470	650
46.25	420	640	46.25	360	470
43.75	290	500	43.75	310	410
41.25	200	330	41.25	250	330
38.75	130	200	38.75	220	280
36.25	80	140	36.25	200	260
33.75	40	90	33.75	170	230
31.25	30	70	31.25	140	210
28.75	20	60	28.75	130	190
26.25	20	60	26.25	120	170
23.75	30	60	23.75	100	170
21.25	30	70	21.25	90	160
18.75	30	80	18.75	70	160
16.25	20	80	16.25	60	150
13.75	20	80	13.75	50	140
11.25	10	90	11.25	50	140
8.75	20	100	8.75	60	140
6.25	40	110	6.25	70	150
3.75	60	130	3.75	70	150
1.25	70	140	1.25	70	150